Quaternary Science Reviews 261 (2021) 106922

Contents lists available at ScienceDirect

Quaternary Science Reviews

journal homepage: www.elsevier.com/locate/quascirev

A maximum rupture model for the central and southern Cascadia subduction zone—reassessing ages for coastal evidence of megathrust earthquakes and tsunamis

Alan R. Nelson [a, 1, *], Christopher B. DuRoss [a], Robert C. Witter [b], Harvey M. Kelsey [c], Simon E. Engelhart [d], Shannon A. Mahan [e], Harrison J. Gray [e], Andrea D. Hawkes [f], Benjamin P. Horton [g], Jason S. Padgett [c, d]

[a] U.S. Geological Survey, Geologic Hazards Science Center, Golden, CO; PO Box 25046, MS 966, Denver, CO, 80225, USA
[b] U.S. Geological Survey, Alaska Science Center, Anchorage, AK, 99508, USA
[c] Department of Geology, Humboldt State University, Arcata, CA, 95524, USA
[d] Department of Geography, Durham University, Durham, DH1 3LE, UK
[e] U.S. Geological Survey, Geosciences and Environmental Change Science Center, Denver Federal Center, Denver, CO, 80225, USA
[f] Earth and Ocean Sciences, Center for Marine Science, University of North Carolina Wilmington, Wilmington, NC, 28403, USA
[g] Earth Observatory of Singapore and Asian School of the Environment, Nanyang Technological University, 639798, Singapore

ARTICLE INFO

Article history:
Received 8 December 2020
Received in revised form
28 March 2021
Accepted 31 March 2021

Handling Editor: Giovanni Zanchetta

Keywords:
Paleoseismology
Earthquake and tsunami hazards
Radiocarbon dating
Maximum rupture model
Megathrust earthquake recurrence
Earthquake contacts
Bayesian age models

ABSTRACT

A new history of great earthquakes (and their tsunamis) for the central and southern Cascadia subduction zone shows more frequent (17 in the past 6700 yr) megathrust ruptures than previous coastal chronologies. The history is based on along-strike correlations of Bayesian age models derived from evaluation of 554 radiocarbon ages that date earthquake evidence at 14 coastal sites. We reconstruct a history that accounts for all dated stratigraphic evidence with the fewest possible ruptures by evaluating the sequence of age models for earthquake or tsunami contacts at each site, comparing the degree of temporal overlap of correlated site age models, considering evidence for closely spaced earthquakes at four sites, and hypothesizing only maximum-length megathrust ruptures. For the past 6700 yr, recurrence for all earthquakes is 370–420 yr. But correlations suggest that ruptures at ~1.5 ka and ~1.1 ka were of limited extent (<400 km). If so, post-3-ka recurrence for ruptures extending throughout central and southern Cascadia is 510–540 yr. But the range in the times between earthquakes is large: two instances may be ~50 yr, whereas the longest are ~550 and ~850 yr. The closely spaced ruptures about 1.6 ka may illustrate a pattern common at subduction zones of a long gap ending with a great earthquake rupturing much of the subduction zone, shortly followed by a rupture of more limited extent. The ruptures of limited extent support the continued inclusion of magnitude-8 earthquakes, with longer ruptures near magnitude 9, in assessments of seismic hazard in the region.

1. Introduction

Mitigating risk from Earth's greatest (magnitude >8.5) earthquakes and their accompanying tsunamis, as have occurred at subduction zones in Sumatra (2004), Chile (2010), and Japan (2011), requires forecasts based on the recurrence and magnitude of past events. Written history, however, is an inadequate basis from which to forecast the greatest earthquakes and tsunamis at subduction zones (e.g., Sawai et al., 2012; Goldfinger et al., 2013; Philibosian and Meltzner, 2020). Dating prehistoric coastal evidence of such past events remains the primary basis for measuring the recurrence of the greatest earthquakes (Satake and Atwater, 2007; Shennan et al., 2014; Moernaut et al., 2018; Sawai, 2020). Estimating rupture length—a proxy for earthquake magnitude—through correlation of dated evidence of earthquakes along strike has proved problematic due to many dating uncertainties about the times of prehistoric earthquakes (Garrett et al., 2016; Clark et al., 2019; Philibosian and Meltzner, 2020). As elsewhere, along the coasts of

* Corresponding author.
E-mail address: anelson@usgs.gov (A.R. Nelson).
[1] Retired (alannels@gmail.com).

https://doi.org/10.1016/j.quascirev.2021.106922

the Cascadia subduction zone (Fig. 1) the paucity, uncertainty in stratigraphic context, imprecision, and uncertain accuracy of ages for earthquake evidence (almost entirely ^{14}C ages) used to infer the along-strike extent of ruptures (e.g., Nelson et al., 1995; Atwater and Hemphill-Haley, 1997; Nelson et al., 2006; Peterson et al., 2013; Sherrod and Gomberg, 2014; Hutchinson and Clague, 2017; Padgett et al., 2021) have hindered deciphering the variability in recurrence and magnitude needed to accurately model megathrust slip budgets at Cascadia (e.g., Witter et al., 2012; Goldfinger et al., 2012; Wang and Trehu, 2016; Priest et al., 2017), and so assess the region's seismic hazard (Frankel et al., 2015; Petersen et al., 2020). A closely interrelated issue is that thresholds for the creation and preservation of coastal earthquake and tsunami evidence for events of differing magnitude vary from site to site along the subduction zone (Nelson et al., 1995, 1996, 2006, 2020a; Atwater and Hemphill-Haley, 1997; Goldfinger et al., 2012, 2016; Atwater and Griggs, 2012; Witter et al., 2012; Graehl et al., 2014; Priest et al., 2017).

When faced with such intractable uncertainties about megathrust earthquake dating, creation and preservation thresholds, and the completeness of coastal stratigraphic sequences, one approach that can provide useful constraints on seismic hazard assessment involves developing a maximum rupture model (MRM; Fig. 2; Scharer and Yule, 2020) through correlating dated earthquake evidence from site to site. An MRM is but one of a spectrum of possible earthquake rupture models that incorporates the fewest

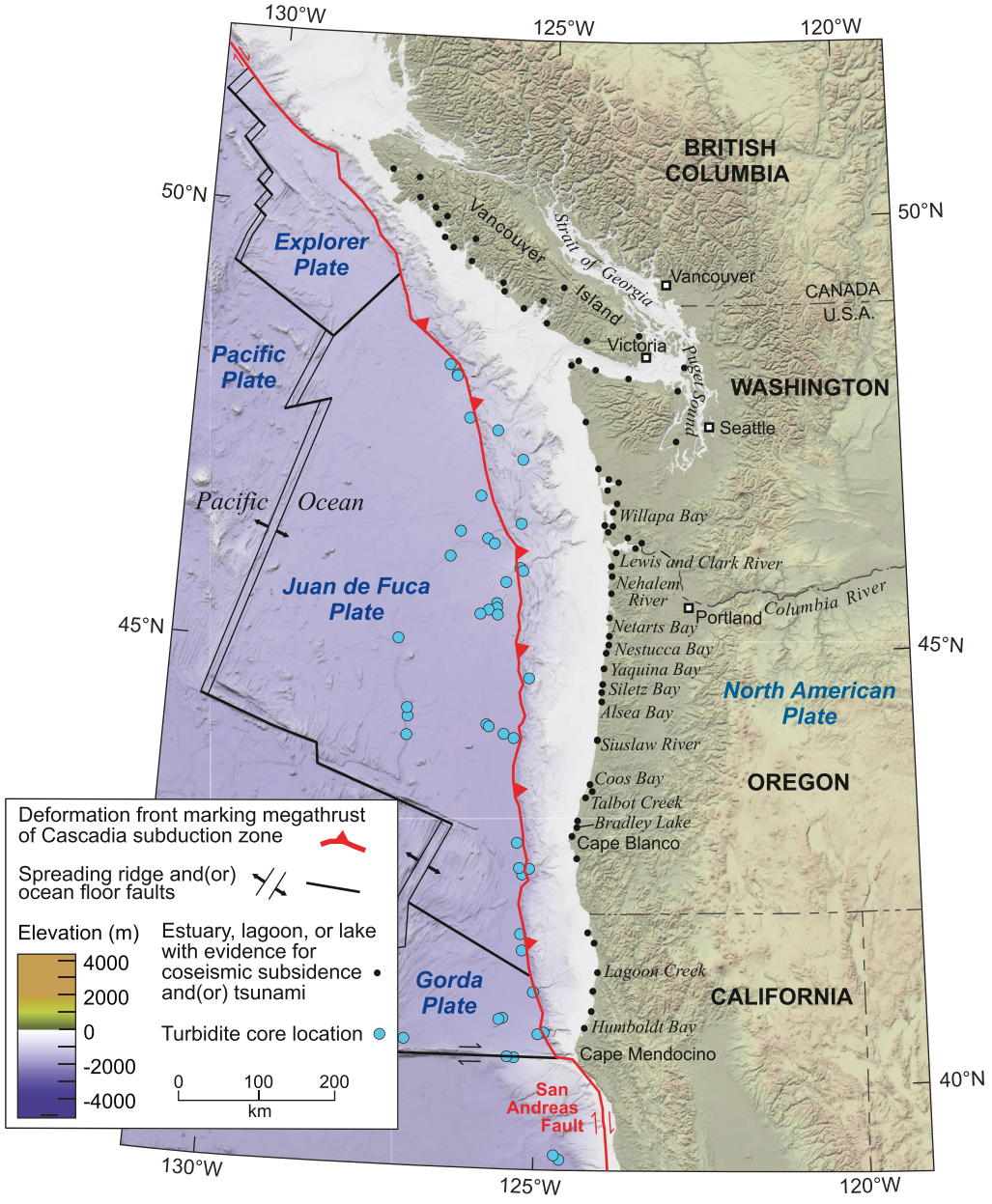

Fig. 1. Physiography and major features of the Cascadia subduction zone showing the location of Bradley Lake and the tidal wetland sites of this study (labeled black dots, Fig. 2) along the coasts of Oregon and northern California (base map data source: GEBCO Compilation Group [2019] GEBCO, 2019 Grid, https://doi.org/10.5285/836f016a-33be-6ddc-e053-6c86abc0788e). The deformation front of the subduction-zone megathrust fault on the ocean floor (red barbed line) is near the bathymetric boundary between the continental slope and abyssal plain. Unlabeled dots mark other estuaries, lagoons, or lakes with evidence for coastal subsidence and (or) tsunamis, and marine turbidites accompanying subduction-zone earthquakes. (For interpretation of the references to colour in this figure legend, the reader is referred to the Web version of this article.)

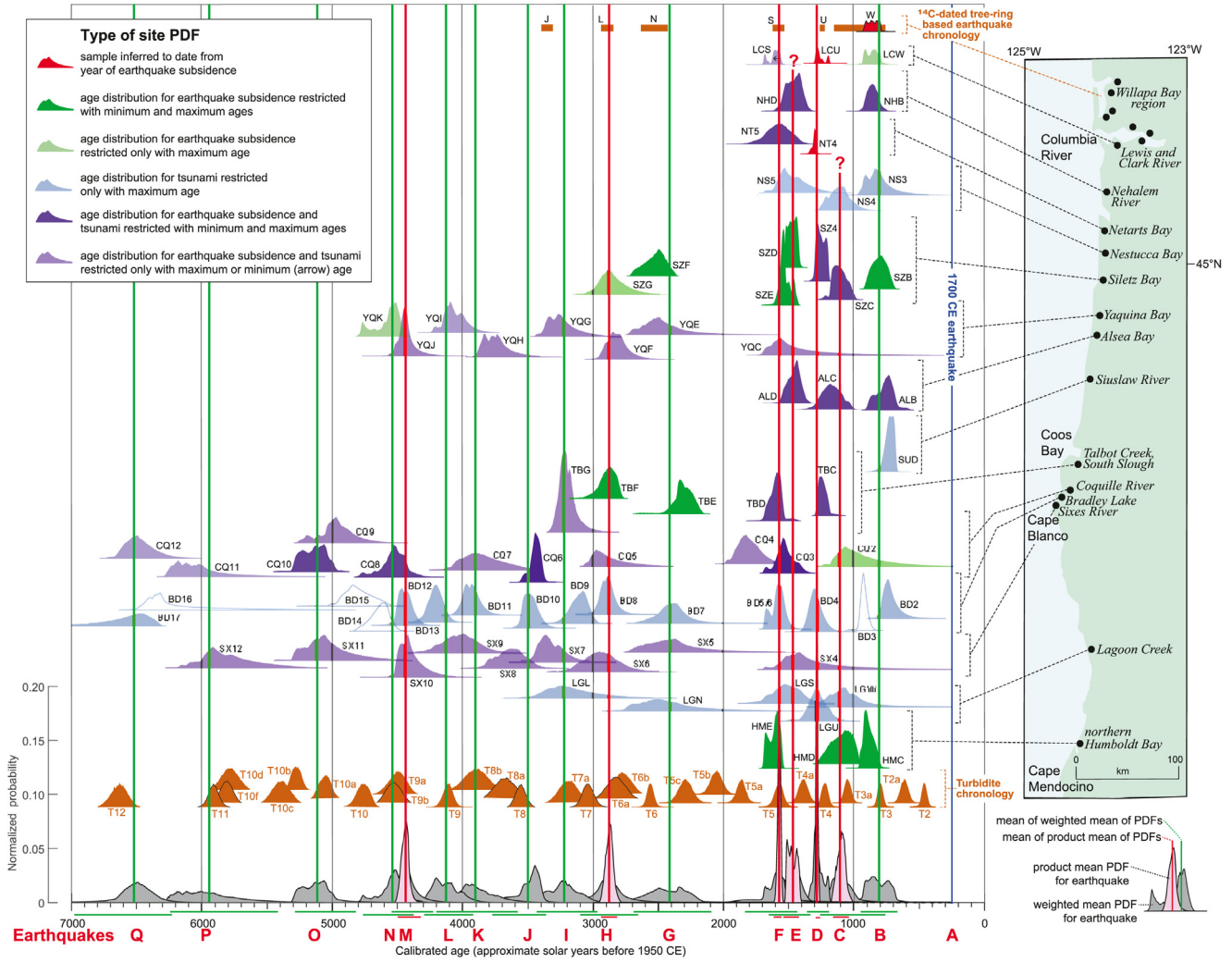

Fig. 2. Radiocarbon-based age models (probability density functions, or PDFs) for evidence of great earthquakes and their accompanying tsunamis that predate the great earthquake of 1700 CE (blue vertical line; Atwater et al., 2005) at 14 sites (site map at right) between the Columbia River and Cape Mendocino, California. PDFs for earthquakes at each site calculated through evaluating 554 ^{14}C ages (Tables S3A-S3G) with the sequence feature of OxCal (Bronk Ramsey 2008; 2009a). Labels used by original investigators for PDFs (dated contacts) at each site are listed in Table 2. We developed a maximum rupture model (MRM) for this region by assigning site PDFs to 16 earthquakes (B-Q, red labels at base), and then calculating weighted (based on the quality of ^{14}C ages, Table 2) mean PDFs (gray distributions at base) and product PDFs (pink distributions) for each earthquake (Figs. 4–6, and S4A-S4E; e.g., Biasi and Weldon, 2009; DuRoss et al., 2011). We show product PDFs only for earthquakes (C, D, E, F, H, and M) whose site PDFs closely coincide (Table 1), from which we infer that all site PDFs for those earthquakes are equally valid estimates of earthquake age. For other earthquakes, with broader less coincident site PDFs, we infer only that the times of earthquakes are within the range of their weighted mean PDFs. Vertical lines mark means of the weighted mean PDFs (green) and product PDFs (red). Bars below earthquake PDFs are 95% confidence limits for mean PDFs (upper green row) and product PDFs (lower red row). The PDFs at Lewis and Clark River are calibrated distributions for a single age for each of three earthquakes, not an OxCal-modeled PDF as at other sites. Age intervals shown only for visual comparison for earthquakes in the Willapa Bay region (upper brown bars), are mostly based on the ages of rings from tree stumps inferred to have died shortly after earthquake subsidence (Atwater et al., 2004). The probability distribution in front of interval W (red), is a more precise estimate calculated from the average of three ages reported by Atwater and Griggs (2012, p. 22; Atwater, 2020). PDFs for marine turbidites offshore (lower brown PDFs, not to same vertical scale as other PDFs) are those of Goldfinger et al. (2012; from their Fig. 54B), calculated by combining distributions for ^{14}C ages for the correlated turbidites in many cores. (For interpretation of the references to colour in this figure legend, the reader is referred to the Web version of this article.)

number of earthquakes consistent with all dated paleoseismic evidence. It is universally recognized that correlation of megathrust earthquakes dated with broad age distributions at a series of sites cannot distinguish near full-subduction-zone-margin ruptures from serial ruptures of more limited coastal extent spaced minutes to decades apart (e.g., Atwater et al., 1991; Clarke and Carver, 1992; Nelson, 1992; Clague, 1997; Nelson et al., 2006). For this reason, an MRM approach is implied by most past correlations of earthquake and tsunami evidence at Cascadia, as well as at other subduction zones (Shennan et al., 2014; Clark et al., 2019; Sawai, 2020). For example, Hutchinson and Clague (2017) essentially hypothesize an MRM in asking of the coastal record of megathrust earthquakes in northern Cascadia, "Were they all giants?" Earthquake recurrence intervals calculated from an MRM for a fault system yield only maximum estimates of recurrence. An MRM is an end-member model of earthquakes with the greatest magnitudes and, presumably, the greatest rupture extents along a subduction zone; at the other end of the spectrum are lower magnitude megathrust earthquakes with ruptures of much more limited extent.

Here, we develop an MRM for the central and southern Cascadia subduction zone through a four-step process (discussed in following sections). First, we evaluate 554 ^{14}C ages, including 168 new unpublished ages, for stratigraphic contacts inferred to record regional coseismic coastal subsidence or tsunamis during great

(magnitude >~8.5) megathrust earthquakes of the past 6700 yr at 14 coastal sites between the Columbia River and Humboldt Bay, California (Fig. 2). Our evaluation includes the dating of the 13 tsunamis that inundated Bradley Lake in southern Oregon (Kelsey et al., 2005; Nelson et al., 2006; Witter et al., 2012, 2013; Priest et al., 2017), one of the longest and most complete of Cascadia's coastal records of megathrust earthquakes. Because all dated samples from the lake are detrital plant macrofossils found at the tops of tsunami deposits and emplaced by processes different from the processes of dated fossil emplacement at the other 13 estuary and lagoon tidal sites, at Bradley Lake we date events only with maximum ages, whereas we use maximum and minimum ages for many contacts at the tidal sites. We do not evaluate ^{14}C ages for evidence of the most recent Cascadia megathrust earthquake in 1700 CE (Satake et al., 2003; Atwater et al., 2005) because all but a very few of its ^{14}C ages on counted tree-ring samples (e.g., Atwater et al., 2004; Atwater, 2020) cannot usefully date it due to the plateau in the ^{14}C calibration curve during the past 400 yr (Nelson et al., 1995; Hutchinson and Clague, 2017). Second, from a subset (22%) of evaluated ages that most closely limit the times contacts formed, we calculate probability density function (PDF) distributions for the ages of earthquake and (or) tsunami contacts at each site. Third, after making assumptions about the sequences of site PDFs, comparing the degree of temporal overlap among PDFs, and considering stratigraphic evidence at four key sites; we build an MRM consisting of 16 megathrust earthquakes through correlation of PDFs from site to site. Note that no site has a complete record of all 16 earthquakes (Fig. 2). Fourth, for each MRM earthquake we consider the consistency of our PDF correlations and calculate age intervals. From the MRM plus the addition of the 1700 CE earthquake (which we assume ruptured throughout central and southern Cascadia, Satake et al., 2003, Table 1), we then calculate earthquake recurrence over varying time periods. Our MRM features four more great megathrust ruptures than first proposed from the coastal record in southern Cascadia (Kelsey et al., 2002, 2005; Witter et al., 2003; Witter and Kelsey, 2004; and Nelson et al., 2006), at least two of which may have been of limited extent. It also identifies times between earthquakes that range from near half a century to close to a millennium.

2. Dating and age modeling

2.1. ^{14}C dating Bradley Lake disturbance events

Of the 17 disturbances that interrupt Bradley Lake's mostly laminated mud stratigraphy (Kelsey et al., 2005), dated by accelerator mass spectrometer (AMS) ^{14}C dating (Supplemental Data, Table S1), 13 record tsunami inundations accompanying Cascadia megathrust earthquakes. The four other disturbance events, inferred to be caused by strong shaking without tsunami inundation in the lake, may or may not have been caused by megathrust earthquakes (Kelsey et al., 2005). At Bradley Lake, we sampled multiple types of macrofossils in 20 of 78 existing samples (refrigerated after core splitting in 1995 and frozen <3 yr later) from 10 of the 26 cores from the lake, and sampled similar materials in 7 new core samples in conjunction with sampling sandy tsunami deposits for optically stimulated luminescence (OSL) and infrared stimulated luminescence (IRSL) dating. Because of sample requirements for AMS ^{14}C dating in the late 1990s, most of the samples dated previously consisted of mixtures of detrital fossils, such as conifer needles, twigs, seeds, and aquatic moss stems (Figs. 3, S1A-S1C), from muddy beds containing coarse organic debris. These materials were deposited through settling hours to days following lake disturbance by tsunami inundation (Table S1; Fig. 3; debris-rich mud facies of Kelsey et al., 2005).

We were far more selective in choosing materials for the 40 new ^{14}C samples (in a total of 140 ages from the lake, Table S1), whose weights were less than a fifth (~0.05–0.2) of those of the samples analyzed in the 1990s. Nevertheless, the new ages on different materials range in age as widely as do the original ages on much heavier mixtures of a variety of debris types (Figs. 3, S1A, S1B, and S1C), and the new ages are not consistently the youngest for any disturbance event. For example, <0.1 mm diameter, semi-translucent rootlets and strands of preserved herbaceous tissue, which we judged most likely to be fragile and therefore potentially the youngest sample material, gave the youngest ages for some disturbance events but the oldest for others. In contrast, spruce needles and wood fragments, materials commonly assumed to be the most likely to be older than earthquake and tsunami contacts at tidal sites (e.g., Witter et al., 2009; Milker et al., 2016; Nelson et al., 2020a; Kelsey and Witter, 2020), gave ages as young as any others for six lake disturbance deposits (disturbance events 2, 3, 7, 12, 15, and 17, Table S1). The 0.3–1.5 m thick, unconsolidated beds of forest litter and other coarse organic debris that we observed at water depths of 1–2 m along the shores of Bradley Lake apparently accumulate such materials over decades to hundreds of years (Goldfinger et al., 2012; Witter et al., 2012). Such debris was distributed and redeposited throughout the lake each time tsunamis or strong shaking disturbed the lake.

We used OxCal Bayesian stratigraphic-ordering software (version 4.4; Bronk Ramsey, 2008; 2009a) to compute a series of PDFs for 16 pre-1700 CE disturbance events (13 partly caused by tsunami inundation following a Cascadia megathrust earthquake) in Bradley Lake described by Kelsey et al. (2005; Fig. 2). Initial modeling consisted of outlier analyses (methods of Bronk Ramsey, 2009b; examples in the supplemental data of Witter et al., 2019; Nelson et al., 2020a) starting with all ages from the lake and mean sediment thicknesses between events in the axial lake cores of Kelsey et al. (2005, their Table 4). Most ages were grouped into OxCal phases (groups consisting of unordered samples) for each disturbance event.

Although many previous studies of Cascadia's earthquake prehistory have averaged ^{14}C ages for the same events under the assumption that dated materials of similar stratigraphic position and age are from the same age population (e.g., Witter et al., 2003; Kelsey et al., 2005; Nelson et al., 2006; Hutchinson and Clague, 2017), the variety of materials dated at Bradley Lake and our demonstration of their range in ages makes this assumption unlikely (e.g., Goldfinger et al., 2012; Johnstone et al., 2019; Nelson et al., 2020a; Streig et al., 2020; Scharer and Yule, 2020). Instead, at Bradley Lake we use the youngest maximum ^{14}C age for each disturbance event (Table S1) as the best estimate of the time of disturbance. We then substitute these youngest maximum ages for the average ages in the original OxCal stratigraphic-ordering, age model (Bronk Ramsey, 2008; 2009a; V-sequence model) for the lake disturbance events of Kelsey et al. (2005; OxCal code in Nelson et al., 2020c) to obtain a PDF for each event. Because calibrated distributions for individual ages span longer time intervals than averaged ages, our PDFs calculated using the single (youngest) age span longer time intervals than the averaged (2–4, Table S1) ages of Kelsey et al. (2005) for the same events. The Kelsey et al. (2005) model additionally constrains (only slightly) the age ranges for events with varved-based, sedimentation-rate estimates for the number of years between events (with assumed errors of ±25%; Kelsey et al., 2005, their Table 4 and Fig. 14). Although their PDF age models are shown on Fig. 2, we do not include PDFs for disturbance events 3, 14, 15, and 16 in our correlation of earthquake and tsunami evidence because Kelsey et al. (2005) were uncertain whether or not the strong shaking without tsunami inundation recorded by these events was caused by megathrust earthquakes.

Table 1
Data for megathrust earthquakes in a maximum rupture model for central and southern Cascadia.

Earthquake (Fig. 2)	Age interval (yr BP)[a]	Rupture length (km)[b]	Sequence of correlated site PDFs[c]	Overlap coefficient[d] Mean	Range	Agreement index (percent)[e]	Chi-squared[f]
A	250 assumed	–	No ages for contacts considered in this paper	–	–		–
B	930–650	600	LCW(0.6)-NHB*(0.6)-NS3(0.4)-SZB (0.6)-ALB (0.6)-SUD*(0.6)-BD2 (0.4)-HMC(0.6)	0.45	0.04–0.83	16 (25)	16.4 (14)
C	***1160–1040***	400	NS4(0.4)-SZC (0.8)-ALC (0.6)-CQ2 (0.4)-LGW (0.2)-HMD(0.6)	0.65	0.36–0.86	160 (28)	1.7 (11)
D	***1295–1270***	500	LCU(1.0)-NT4*(1.0)-SZ4 (0.6)-TBC*(0.4)-BD4 (0.4)-LGU (0.2)	0.46	0.05–0.83	77 (28)	7.0 (11)
E	***1525–1420***	350	NHD (0.6)-NS5(0.4)-SZD (0.4)-ALD (0.6)-CQ3 (0.6)-LGS (0.2)	0.61	0.41–0.84	113 (28)	4.0 (11)
F	***1600–1560***	600	LCS(0.6)-NT5 (0.8)-SZE*(0.8)-YQC (0.2)-TBD (0.6)-CQ4*(0.4)-BD5/6 (0.4)-SX4 (0.4)-HME (0.6)	0.41	0.06–0.89	47 (23)	12.6 (16)
G	2680–2090	500	SZF (0.6)-YQE (0.2)-TBE*(0.6)-BD7 (0.2)-SX5 (0.2)-LGN (0.2)	0.57	0.11–0.85	79 (28)	6.9 (11)
H	***2935–2825***	400	SZG (0.4)-YQF (0.2)-TBF(0.4)-CQ5 (0.4)-BD8 (0.4)-SX6 (0.4)	0.63	0.48–0.78	182 (28)	1.3 (11)
I	3455–2965	350	YQG (0.2)-TBG (0.4)-BD9*(0.2)-SX7 (0.4)-LGL (0.2)	0.50	0.21–0.73	75 (31)	5.4 (9.5)
J	3785–3380	400	CQ6 (0.6)-BD10 (0.4)-SX8*(0.4)	0.41	0.21–0.73	67 (40)	3.2 (6.0)
K	4200–3580	200	YQH (0.2)-CQ7 (0.4)-BD11 (0.4)-SX9 (0.4)	0.43	0.16–0.59	67 (35)	4.8 (7.8)
L	4295–3915	200	YQI (0.2)-BD12 (0.2)	0.23	–	74 (50)	2.9 (3.8)
M	***4495–4305***	200	YQJ (0.2)-BD13 (0.2)-SX10 (0.2)	0.80	0.78–0.84	155 (40)	0.5 (6.0)
N	4770–4370	200	YQK (0.2)-CQ8 (0.6)	0.78	–	140 (50)	<0.1 (3.8)
O	5295–4810	40	CQ10 (0.6)-SX11 (0.2)	0.68	–	123 (50)	<0.1 (3.8)
P	6255–5420	40	CQ11 (0.4)-SX12 (0.2)	0.45	–	87 (50)	1.8 (3.8)
Q	7005–6255	40	CQ12 (0.4)-BD17 (0.2)	0.68	–	138 (50)	<0.1 (3.8)

[a] Confidence interval (95%) of product PDF for earthquakes C, D, E, F, H, and M (in bold italics), and of weighted mean PDF for other earthquakes (Table 3).
[b] Apparent distance on Fig. 2 among correlated site PDFs for each earthquake rounded to the nearest 50 km. All distances, except those for earthquakes C and E, are inferred to be minimums.
[c] PDFs for each maximum rupture model earthquake (Fig. 2) are listed from north to south. Quality weighting factor for site PDFs used in weighted mean PDFs (Table 2) is within parentheses. Site PDFs marked with asterisks are those whose individual agreement indices (An, methods of Bronk Ramsey, 2001; 2009a) fall below the 60% acceptable limit in a combined analysis of site PDFs (methods of Bronk Ramsey, 2001; 2009a) for each earthquake (see Figs. 4–6, and S4A-S4E).
[d] Average and range of overlap coefficients (e.g., Biasi and Weldon, 2009) for all pairs of correlated site PDFs for each earthquake in the maximum rupture model.
[e] Agreement index (Acomb) for combined site PDFs (methods of Bronk Ramsey, 2001; 2009a) for each earthquake in the maximum rupture model; minimum acceptable index in parentheses.
[f] Value of T statistic for combined site PDFs (methods of Bronk Ramsey, 2001; 2009a) with 5% value (in parentheses) needed to reject the hypothesis that correlated PDFs are the same age. Chi-squared values show that, for PDFs assigned to each earthquake, the differing earthquake hypothesis fails at the 5% level, except for earthquake B.

In any case, if we had included PDFs for disturbance events 3, 14, 15, and 16 in our correlations of PDFs for earthquake and tsunami evidence (discussed below), it would have reduced the consistency of our MRM because the PDFs for these disturbance events provide only poorly limiting maximum ages for MRM earthquakes.

2.2. Attempted luminescence dating of Bradley Lake tsunami deposits

In an attempt to confirm our modeled ages (PDFs) for Bradley Lake disturbance events, we used luminescence techniques to date tsunami deposits coinciding with seven of the most extensive disturbance events (Table S2; Mahan et al., 2021). We extracted quartz and K-feldspar from beds of very fine to medium sand using standard preparation techniques for luminescence dating (Gray et al., 2015). Previously, Ollerhead et al. (2001) tried to date tsunami deposits at Bradley Lake using infrared stimulated luminescence (IRSL) techniques. Following fading corrections, these authors found that IRSL ages for two of their samples were similar to ^{14}C ages from the same levels in lake cores, whereas ages for three other samples were large overestimates.

We attempted optically stimulated luminescence (OSL) dating of the seven tsunami deposits using single aliquots of quartz, as grains dated by this method are more likely to be reset than are those measured using IRSL. However, our preliminary tests demonstrated that the quartz has poor luminescence characteristics resulting in unacceptable dose recovery ratios. In particular, infrared depletion tests suggest pervasive contamination of the quartz with probable feldspar inclusions (Mahan et al., 2021). We then tried IRSL dating of ~10 sand grains (per aliquot) to isolate populations of fully reset grains, which could be statistically resolved with minimum age methods (Galbraith and Roberts, 2012). We used a standard single aliquot regeneration protocol (Murray and Wintle, 2003) with optical excitation at 1.4eV and measured the emission at ~3eV following Ollerhead et al. (2001). To confirm our IRSL analyses, we conducted fading tests over 48 h using corrections following Huntley and Lamothe (2001), as well as dose recovery tests.

Despite these efforts, the variable luminescence characteristics of our IRSL samples (Mahan et al., 2021), and their highly inconsistent ages with respect to ^{14}C ages from the same levels in the cores, suggest that they contain sand grains of widely varying age. Samples P1 and T8 exceed the ^{14}C ages from the same levels in the cores by 1000–1500 yr, whereas samples P2, P3, and P6 exceed nearby ^{14}C ages by ~10,000 yr (Table S2). As did Ollerhead et al. (2001), we infer that the seriously overestimated ages are the result of incomplete resetting of grains due to inadequate sunlight

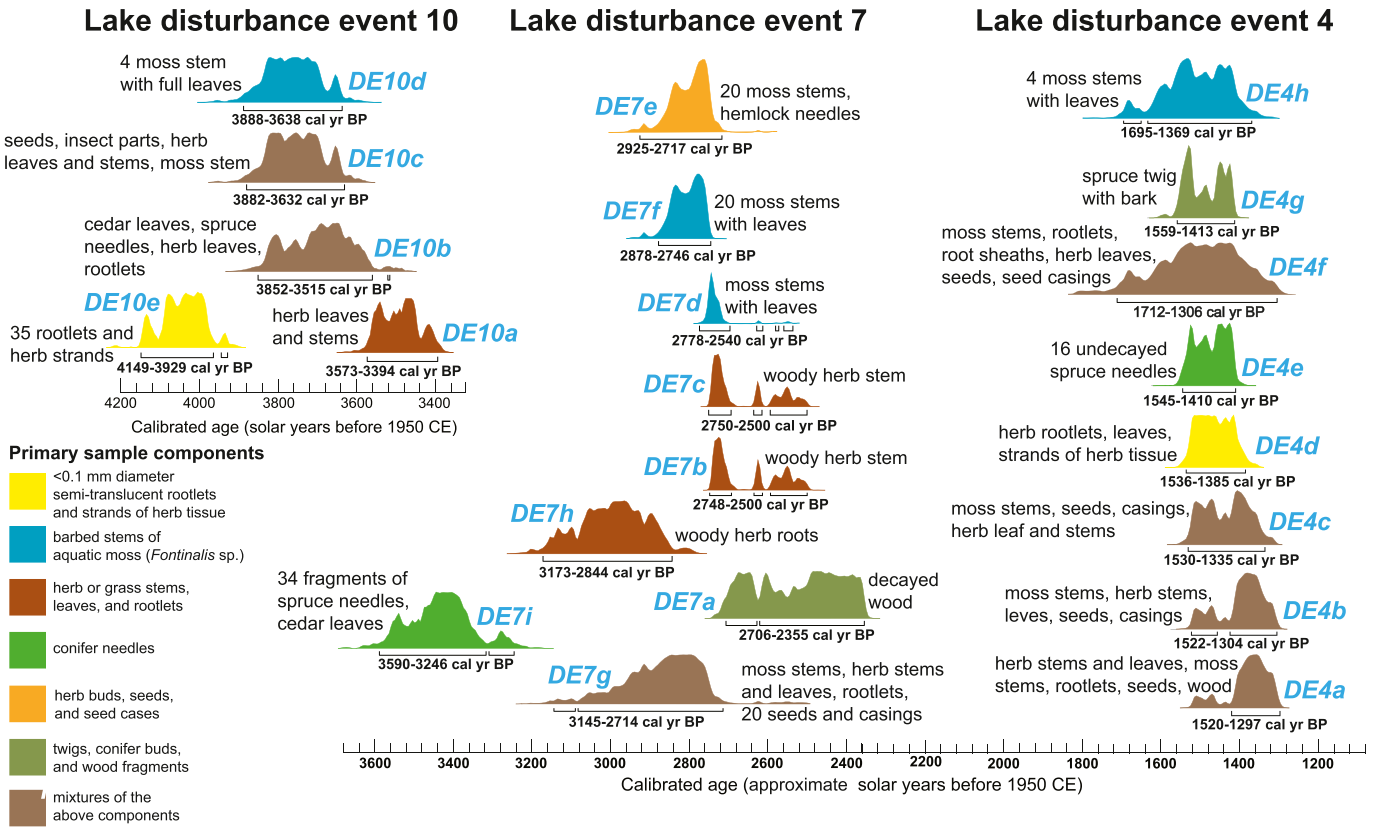

Fig. 3. Comparison of calibrated ^{14}C-age probability distribution functions for individual ages on different materials for three Bradley Lake disturbance events (methods of Bronk Ramsey 2009a; 2009b; distribution labels and other details in Table S1). Brackets and intervals beneath distributions show 95% confidence intervals on ages. Summaries of dated materials are placed next to the distributions; blue labels identify distributions for each age on Table S1. Wider distributions, especially those on mixtures of different materials, are for the ^{14}C ages of Kelsey et al. (2005, their Table 4). Because our unpublished ^{14}C ages on much smaller samples of more carefully selected materials are not consistently younger than published ages, we infer that the ages of the variety of organic materials in disturbance event deposits span decades to hundreds of years. Similar figures for all other ages from Bradley Lake are in Figs. S1A-S1C. (For interpretation of the references to colour in this figure legend, the reader is referred to the Web version of this article.)

exposure. This could be the result of tsunamis inundating the lake at night, extremely turbid water during inundation, or, most likely, to very old sediment being eroded through tsunami scour prior to deposition in Bradley Lake (Ollerhead et al., 2001). In contrast, IRSL samples P4 and P5 appear to underestimate their matching ^{14}C ages (Table S2). A factor here may be the phenomena of anomalous fading, a property of feldspar IRSL where quantum tunneling of trapped electrons causes a decrease in IRSL with time and a resulting age underestimation. However, our 48-h fading tests did not reveal a significant decrease in IRSL, instead producing negative or zero g-values. If anomalous fading occurred in these samples, the effect is not detectable using this method. The only sample with an IRSL age consistent with adjacent ^{14}C ages is X7, but its luminescence characteristics do not distinguish it from the other samples with unreliable IRSL ages (Mahan et al., 2021).

2.3. ^{14}C dating earthquake and tsunami evidence at tidal wetland sites

To develop PDFs for contacts marking earthquakes (and their tsunamis) at tidal wetland sites, we reevaluated 330 previously published ^{14}C ages from the 13 sites and dated 128 new samples from 6 of the sites (Fig. 2; Tables S3A-S3G). Sites evaluated were selected based on the detail and strength of their stratigraphic evidence for earthquake subsidence and (or) tsunami deposition, the areal extent of their evidence, and the number and quality of their ages constraining the times of events. For example, we generally did not evaluate sites with dated contacts identified in only a few cores and (or) contacts dated with only 1–2 maximum ^{14}C ages with large errors (e.g., Peterson and Cruikshank, 2011; Minor and Peterson, 2016). We collected and sampled new cores and (or) exposures at five sites (Lewis and Clark River, Netarts Bay, Siletz Bay, Alsea Bay, and Coquille River; Fig. 2) and resampled existing cores at Talbot Creek. Methods used in the selection of materials for the new unpublished ^{14}C ages are discussed in Kemp et al. (2013), Nelson et al. (2020b), Kelsey and Witter (2020), and Ishizawa et al. (2020). For 20 of 26 contacts for which we obtained one or more new ages, the new ages more tightly constrained modeled contact ages.

For 12 of the 13 tidal sites, we used OxCal software (version 4.4; Bronk Ramsey, 2008; 2009a) to develop a series of PDFs for earthquake and (or) tsunami evidence at each site (Fig. 2). For most sites, initial modeling consisted of outlier analyses (Bronk Ramsey, 2009b) starting with all ages, most grouped into OxCal phases above and (or) below stratigraphic contacts inferred to mark earthquakes and tsunamis. In the series of age models, we then successively eliminated ages that were obvious outliers or that we interpret to be less accurate minimum or maximum estimates of the times that contacts marking earthquakes and (or) tsunamis formed (Tables S3A-S3G; e.g., Milker et al., 2016; Witter et al., 2019; Nelson et al., 2020a; Kelsey and Witter, 2020).

To be consistent with our reasoning above for selecting the youngest maximum ages for Bradley Lake events, for our final modeled age distributions for each of the 12 tidal sites we used an

OxCal sequence (non-outlier) analysis model with only the closest (youngest) maximum age, and (or) the closest (oldest) minimum age (Tables S3A-S3G) to calculate a PDF for each contact inferred to record the time of an earthquake and (or) tsunami (Fig. 2; OxCal code in Nelson et al., 2020c). We base our interpretations of the closest maximum and minimum ages at the 12 tidal sites on the type of dated macrofossil, its orientation, degree of decay and abrasion, host stratigraphic unit lithology, its stratigraphic context relative to adjacent macrofossils and to upper and lower units, and, most importantly, on its calibrated ^{14}C age relative to the ages of samples above and below it. Padgett et al. (2021) compared OxCal sequence modeling results for ages of earthquake contacts at our most southern site, Humboldt Bay, with the results of two other types of Bayesian age models. They concluded that a simple OxCal sequence model gave the most reliable PDFs, as long as limiting minimum and maximum ^{14}C ages for contacts were available.

As elsewhere in Cascadia's coastal sequences (e.g., Nelson et al., 2006; Graehl et al., 2014; Hutchinson and Clague, 2017), at least 80% of the ages from the 13 tidal sites are on detrital macrofossils that yield maximum ages for the times adjacent contacts formed. OxCal modeling of PDFs at tidal sites is more complex than at Bradley Lake, however, because 30% of tidal PDFs are restricted with minimum as well as maximum ages (Fig. 2; Tables S3A-S3G). For example, usually growth-position rhizomes (below ground stems), especially those of *Triglochin maritima* with the bases of its decay-resistant leaves still attached, provide unambiguous minimum ages for underlying contacts (e.g., Tables S3A, S3C, S3D, and S3E). In such cases, however, if a dated rhizome or other plant part grew many decades to centuries after an earthquake, the resulting PDF could largely postdate the time of the earthquake, especially in cases where a close maximum age restricted the PDF. Rarely, we infer from the sequence of ages on adjacent samples that the rhizomes of plants younger than a contact grew down into the peaty unit just below a contact and so provide minimum ages for the contact despite being found below it (e.g., Nelson et al., 2020b).

For the northernmost tidal wetland site, Lewis and Clark River (Fig. 2), although we list published and unpublished ages for that site in Table S3A, we used only three calibrated-age probability distributions for three new unpublished ages to estimate the times of three earthquake contacts. We did not use other ages from this site to model PDFs for contacts because most of the other ages were combined with many others from other sites by Atwater et al. (2004) to develop the age intervals for earthquakes throughout the Willapa Bay-Grays Harbor region (upper brown bars of Fig. 2). Calibrated-age distributions for our three new ages largely overlap the time intervals of Atwater et al. (2004) for the same earthquake contacts.

3. An MRM based on correlation of earthquake and tsunamis contacts

3.1. Model assumptions and criteria

In developing an MRM for central and southern Cascadia based on coastal evidence we make several assumptions and apply various criteria. First, we select the 14 sites of Fig. 2 based on available details of their stratigraphy, the areal extent of their earthquake and (or) tsunami contacts, and the number and quality of ^{14}C ages constraining the times of events. We also assume that the original investigators of each site correctly interpreted each earthquake and (or) tsunami contact as recording a megathrust event (references in Supplemental Data Tables S1, S3A-S3G). For example, Nelson et al. (2020a) evaluated 9–12 tidal contacts of the past 2000 yr in central Oregon but concluded that only one showed evidence sufficient to infer subsidence and a tsunami during a megathrust earthquake. Following Sharer and Yule (2020), by considering the number and approximate age of contacts at each site (excluding the most recent earthquake in 1700 CE) we build our MRM back through time by correlating PDFs for earthquake and tsunami contacts from site to site. PDFs at sites with a sequential number of events are, in most cases, included in the youngest permissible correlations. Unlike Scharer and Yule (2020), however, we do not assume that the sequence of events for any site is complete because of the likelihood of differing creation and preservation thresholds for evidence of different earthquakes and tsunamis at various sites (e.g., Nelson et al., 2006; Witter et al., 2012; Shennan et al., 2016; Dura et al., 2016; Clark et al., 2019). Even for the most recent 2000 yr, all but one of our sites (Siletz Bay, Fig. 2) lacks a contact for at least one of the five earthquakes in our MRM.

In the face of these uncertainties about completeness, in building our MRM we make additional assumptions and consider additional evidence. First, we assume all site contacts of the past 6700 yr on Fig. 2 correlate with (record the same earthquake as) at least one other (an exception is 5-ka-old contact CQ9). Secondly, we assume that the length of each megathrust rupture greatly exceeds the mean distance between sites (~45 km). A third assumption, which supports the second, is that evidence for all site contacts is sufficient to infer that they record megathrust ruptures >200 km long. Such evidence includes distinct changes in tidal lithologies or microfossils across contacts typical of recording >0.5 m of coseismic subsidence, or anomalously sandy deposits laid down by tsunamis extending unusual heights and distances inland from the sea. As discussed below, we also inform our MRM with these types of stratigraphic evidence for closely spaced earthquakes and tsunamis at four key sites (Bradley Lake, Sixes River, Coquille River, and Siletz Bay; Fig. 2).

Other factors that may influence the accuracy of our MRM correlations of site PDFs include differing abundance and types of plant macrofossils in deposits adjacent to earthquake and tsunami evidence (e.g., Kemp et al., 2013; Nelson et al., 2020a; Kelsey and Witter, 2020), differing processes that deposited dated fossils in Bradley Lake compared with processes at tidal sites, differing lengths of site stratigraphic records, differing amounts of time for sediment accumulation at differing rates between earthquakes (e.g., Witter and Kelsey, 2004; Witter et al., 2019; Padgett et al., 2021), and differing amounts of coastal deformation during earthquakes of differing magnitudes (e.g., Nelson et al., 2006; Witter et al., 2012; Milker et al., 2016; Wang and Trehu, 2016; Hutchinson and Clague, 2017; Wirth and Frankel, 2019). As these factors have not been discussed for most earthquakes at most of the sites of Fig. 2, we do not try to assess them for each site in building our MRM.

3.2. Comparison of PDF overlap coefficients

Although of secondary priority to the above criteria in building our MRM, we also employ a simple overlap coefficient that measures the areal overlap of paired site PDFs among the 73 PDFs (Table S4; 100% overlap yields a coefficient of 1.0; e.g., Biasi and Weldon, 2009; DuRoss et al., 2011; Hutchinson and Clague, 2017) to help decide among alternative correlations of PDFs. For example, at Nehalem River (Fig. 2; Nelson et al., 2020a; Table S3B), the PDF for contact NHD only minimally overlaps the PDF for contacts LCS (earthquake F) and LCU (earthquake D) to the north at Lewis and Clark River (overlaps of 0.09 and < 0.01, Table S4; Table S3A). Farther south at Siletz Bay (Engelhart et al., 2013; Witter et al., 2015), earthquake contacts SZD and SZE, separated by decimeters of mud at the Millport Slough site and differing in age by decades (Table S3E; discussed below), show that two separate earthquakes and (or) tsunamis are recorded at this site. For this reason, we

correlate the PDF for contact NHD at Nehalem River, as well as the PDF for contact ALD at Alsea Bay, with the PDF for contacts SZD at Siletz Bay (overlaps of 0.62 and 0.62), rather than with the PDF for contact SZE at Siletz Bay (overlaps of 0.52 and 0.38) and contact LCS at Lewis and Clark River (overlaps of 0.09 and 0.02). In the same way, overlap coefficients lead us to include tsunami contact ALC at Alsea Bay in our correlations for earthquake C rather than for earthquake D, and contact TBC at Talbot Creek with earthquake D rather than with earthquake C.

Although our coefficient comparisons are more quantitative than most approaches used to correlate coastal earthquake evidence at Cascadia (e.g., Nelson et al., 2006; Peterson et al., 2013; Graehl et al., 2014; Milker et al., 2016), we do not apply uniform criteria in comparing coefficients or exclude correlations of PDFs with coefficients below a certain value. For example, at Coquille River, despite the low overlap coefficients for contact CQ4 with PDFs to the north and south (0.11 for TBD and 0.10 for BD5/6) we include it in our correlations for earthquake F even though contact CQ3 has greater overlaps with these adjacent PDFs (Fig. 2). As explained further below, correlating contact CQ3 with earthquake F would isolate contact CQ4 from correlation with any earthquake, an unlikely prospect considering the extent of its tsunami deposit at the Coquille River and the $\leq$2 m of earthquake subsidence inferred across its contact (Witter et al., 2003; Witter and Kelsey, 2004). With our goal of constructing an MRM with the minimum number of ruptures, we follow the same reasoning for contact HMC at Humboldt Bay (Padgett et al., 2021; discussed below).

We make only qualitative visual comparisons among the site PDFs (Fig. 2) and the time intervals for megathrust earthquakes of Atwater et al. (2004) in the Willapa Bay region, and the age model PDFs for the shaking-induced marine turbidites of Goldfinger et al. (2012; brown PDFs on Fig. 2). The ages on which both types of age estimates are based depend on assumptions quite different from those used in our evaluation of ^{14}C ages from lake and tidal wetland sites. Atwater et al. (2004) used OxCal to limit the age ranges for megathrust earthquake contacts by using (1) maximum ages correlated among six sites, as many as 90 km apart, on the rings of trees (inferred to have been killed by earthquake subsidence) a counted number of tree-ring years prior to tree death, (2) detrital plant fossils beneath earthquake contacts, and (3) minimum ages on growth-position rhizomes above contacts (for 2 of 7 contacts).

Goldfinger et al. (2012, Appendix 5; 2016) had a different series of problems in modeling PDFs for turbidites on the continental slope inferred to have been triggered by strong shaking during megathrust earthquakes. They estimated turbidite age by ^{14}C dating foraminifera extracted from hemipelagic sediment a few centimeters below turbidites. In doing so, they had to consider the apparent age of seawater from which the foraminifera extracted their carbon, how the apparent age may have changed as a result of marine current changes during the Holocene, how much time was represented by the hemipelagic sediment that the foraminifera came from, and how much time was represented by the missing hemipelagic sediment just beneath the turbidite that was eroded during its emplacement. They then used OxCal to model age distributions for each turbidite incorporating the sedimentation-rate-based age gaps between selected averaged ^{14}C ages in a manner similar to that used by Kelsey et al. (2005) at Bradley Lake. Although many PDFs for turbidites overlap with the PDFs of the next-oldest and next-youngest turbidite (Fig. 2), Atwater and Griggs (2012) suggest that the 95% confidence interval uncertainties on the PDFs may be greater than presented by Goldfinger et al. (2012).

3.3. Weighting site PDFs based on ^{14}C sample quality

As close inspection of our evaluated ages at the 14 sites shows (Tables S1, S3A-S3G), the quality of radiocarbon-dated materials, in terms of the resulting abilities of their ages to accurately reflect the times of earthquakes, varies greatly. For example, many ages on macrofossils from Bradley Lake disturbance event deposits are tens to hundreds of years older than ages on other fossils from the same bed (Table S1, Figs. 3, S1A-S1C). Many of the ages on detrital fossils that we evaluated from tidal wetland sites show similar discordance in ages for samples from near the same contacts (Tables S3A-S3G). In contrast, we infer that a few ages are on fossils that probably date from the year of an earthquake (Fig. 2). For example, one such age is on four cf. *Schoenoplectus* sp. seeds with delicate, curving bristles still attached to their bases found in fine mud 1 cm above contact LCU at Lewis and Clark River (Soil U, Table S3A). This genus is widespread at the site and the bristles are probably too fragile to have remained attached to the seeds for more than a year. In an attempt to consider the wide range in the ability of the ages used to model site PDFs to closely date earthquakes, we weight each site PDF based on our overall estimate of the quality of its dated samples (Table 2; e.g., Clark et al., 2019). The intent of weighting is to use site PDFs constrained with the highest quality ages to skew our age estimates towards the most likely times of earthquakes.

In our weighting we use a five-point scale to assess (1) the type and (or) probable genus and (or) species (where this can be reasonably inferred) of a dated macrofossil, (2) whether the macrofossil is detrital or in growth position, (3) the macrofossil's degree of decay and preservation, (4) the macrofossil's stratigraphic context, including relative depth above or below an earthquake or tsunami contact, and the lithology and probable genesis of the stratigraphic unit the macrofossil occurs in, and (5) the degree to which the macrofossil's age is consistent with ages on adjacent samples near the same contact and with ages on samples from upper and lower contacts, and the precision of the site PDF. For example, a PDF restricted with ages on the well preserved seeds of common high marsh plants (e.g., *Atriplex* sp., or *Carex* sp.) from the upper 1 cm of peat below a contact, and by growth-position rhizomes of *Triglochin maritima* in fine mud a few centimeters above the contact, would be rated highly (3–4, Table 2), especially if the width of the modeled PDF was narrow and its age range was consistent with maximum and minimum ages for contacts stratigraphically above and below it. In contrast, we rate PDFs constrained with only maximum ages on detrital fossils from above or below contacts lower (1–2), especially if the macrofossils are resistant to decay and transport (conifer needles, aquatic moss stems, twigs, conifer cone bracts) or are found above the contact in high-energy, sandy tsunami deposits rather than in quiet water muddy units deposited following coseismic subsidence.

3.4. Calculating MRM earthquake ages

To estimate ages for the 16 earthquakes (and accompanying tsunamis) in our MRM (Table 1), we calculate mean PDFs (unweighted and weighted) and product PDFs, including single-year mean values (Table 3, Figs. 2, 4–6, and S4A-S4E; methods of Biasi and Weldon, 2009, and DuRoss et al., 2011). Mean earthquake PDFs are summed averages of the site PDFs correlated for each earthquake, but the range of mean PDFs spans the full range of contributing site PDFs. Product earthquake PDFs are the product of correlated site PDFs for each earthquake; they are probabilistic versions of the event windows (the overlapping portions of time intervals for correlated earthquakes) used for decades in prehistoric earthquake correlation (Biasi et al., 2011; e.g., Atwater et al., 2004; Clark et al., 2019; Scharer and Yule, 2020). Product PDFs yield narrower distributions than summed mean PDFs because they emphasize the overlap in site PDFs and give greatest weight to the

Table 2
Relative quality weighting of site PDFs for earthquake and tsunamis contacts at Bradley Lake and 13 tidal wetland sites.

Coastal site	Original site label	PDF	Five groups of quality criteria					Average quality rating	Rounded rating value	0-1 weighting factor (value/5)
(Fig. 2)	for dated contact[a]	label	Macrofossil type	Detrital or growth position	Degree of preservation	Stratigraphic context	Consistency and precision of PDF			
Lewis and Clark River	soil W	LCW	3	1	5	3	4	3.2	3	0.6
	soil U	LCU	5	3	5	5	5	4.6	5	1
	soil S	LCS	3	3	3	3	5	3.4	3	0.6
Nehalem River	contact B	NHB	3	3	3	4	4	3.4	3	0.6
	contact D	NHD	3	3	3	4	3	3.2	3	0.6
Netarts Bay	4 MT	NT4	5	5	5	5	4	4.8	5	1
	5 MT	NT5	4	5	3	4	3	3.8	4	0.8
Nestucca Bay	contact N3	NS3	2	1	3	3	2	2.2	2	0.4
	contact N4	NS4	1	1	3	2	2	1.8	2	0.4
	contact N5	NS5	2	1	3	2	3	2.2	2	0.4
Siletz Bay	contact B	SZB	2	3	3	3	3	2.8	3	0.6
	contact C	SZC	3	4	4	5	4	4	4	0.8
	contact 4	SZ4	2	3	3	3	4	3	3	0.6
	contact D	SZD	3	2	2	2	3	2.4	2	0.4
	contact E	SZE	4	4	3	5	4	4	4	0.8
	contact F	SZF	3	3	3	3	3	3	3	0.6
	contact G	SZG	2	2	3	3	2	2.4	2	0.4
Yaquina Bay	buried soil C	YQC	1	1	2	2	1	1.4	1	0.2
	buried soil E	YQE	1	1	2	2	1	1.4	1	0.2
	buried soil F	YQF	1	1	2	2	1	1.4	1	0.2
	buried soil G	YQG	2	1	1	2	1	1.4	1	0.2
	buried soil H	YQH	2	1	1	2	1	1.4	1	0.2
	buried soil I	YQI	2	1	1	2	1	1.4	1	0.2
	buried soil J	YQJ	2	1	1	2	1	1.4	1	0.2
	buried soil K	YQK	2	1	1	2	1	1.4	1	0.2
Alsea Bay	contact B	ALB	3	3	3	3	3	3	3	0.6
	contact C	ALC	3	3	3	3	3	3	3	0.6
	contact D	ALD	3	3	3	3	4	3.2	3	0.6
Siuslaw River	contact Db	SUD	3	3	3	3	3	3	3	0.6
Talbot Creek, South Slough	contact C	TBC	2	2	2	3	3	2.4	2	0.4
	contact D	TBD	3	2	4	3	4	3.2	3	0.6
	contact E	TBE	3	3	4	2	4	3.2	3	0.6
	contact F	TBF	3	2	3	2	2	2.4	2	0.4
	contact G	TBG	1	2	3	2	1	1.8	2	0.4
Coquille River	buried soil 2	CQ2	2	2	3	2	1	2	2	0.4
	buried soil 3	CQ3	3	2	3	2	3	2.6	3	0.6
	buried soil 4	CQ4	2	3	2	2	2	2.2	2	0.4
	buried soil 5	CQ5	2	1	2	2	1	1.6	2	0.4
	buried soil 6	CQ6	3	2	3	2	3	2.6	3	0.6
	buried soil 7	CQ7	2	2	2	2	2	2	2	0.4
	buried soil 8	CQ8	4	3	4	3	3	3.4	3	0.6
	buried soil 9	CQ9	2	2	2	2	2	2	2	0.4
	buried soil 10	CQ10	3	3	3	3	3	3	3	0.6
	buried soil 11	CQ11	2	2	2	2	2	2	2	0.4
	buried soil 12	CQ12	1	2	2	2	2	1.8	2	0.4
Bradley Lake	DE 2	BD2	2	2	3	1	2	2	2	0.4
	DE 4	BD4	1	2	2	1	2	1.6	2	0.4
	DE 5/6	BD5/6	2	2	1	1	2	1.6	2	0.4
	DE 7	BD7	1	2	1	1	1	1.2	1	0.2
	DE 8	BD8	1	2	2	1	2	1.6	2	0.4
	DE 9	BD9	1	2	2	1	1	1.4	1	0.2
	DE 10	BD10	2	2	1	1	2	1.6	2	0.4
	DE 11	BD11	2	2	1	1	2	1.6	2	0.4
	DE 12	BD12	1	2	1	1	1	1.2	1	0.2
	DE 13	BD13	1	2	1	1	1	1.2	1	0.2
	DE 17	BD17	2	2	1	1	1	1.4	1	0.2
Sixes River	buried soil IV	SX4	2	2	2	1	1	1.6	2	0.4
	buried soil V	SX5	1	2	2	1	1	1.4	1	0.2
	buried soil VI	SX6	2	2	2	2	1	1.8	2	0.4
	buried soil VII	SX7	2	2	2	2	1	1.8	2	0.4
	buried soil VIII	SX8	1	2	2	2	1	1.6	2	0.4
	buried soil IX	SX9	2	2	2	2	2	2	2	0.4
	buried soil X	SX10	2	1	2	1	1	1.4	1	0.2
	buried soil XI	SX11	1	1	2	2	1	1.4	1	0.2
	buried soil XII	SX12	1	1	2	2	1	1.4	1	0.2
Lagoon Creek	sand layer W	LGW	2	1	1	2	1	1.4	1	0.2
	sand layer U	LGU	1	1	1	2	1	1.2	1	0.2
	sand layer S	LGS	1	1	1	2	1	1.2	1	0.2
	sand layer N	LGN	1	1	1	2	1	1.2	1	0.2
	sand layer L	LGL	1	1	1	2	1	1.2	1	0.2

(*continued on next page*)

Table 2 (*continued*)

Coastal site (Fig. 2)	Original site label for dated contact[a]	PDF label	Five groups of quality criteria Macrofossil type	Detrital or growth position	Degree of preservation	Stratigraphic context	Consistency and precision of PDF	Average quality rating	Rounded rating value	0-1 weighting factor (value/5)
northern Humboldt Bay	contact C	HMC	3	3	3	3	4	3.2	3	0.6
	contact D	HMD	3	3	3	2	2	2.6	3	0.6
	contact E	HME	3	3	3	2	3	2.8	3	0.6

We used all information about samples, ages, and the resulting PDFs to group PDFs into five general criteria, and then rounded the average ratings for those criteria to the nearest whole number.
The highest relative weighting for each of the five criteria = 5; the lowest relative weighting = 1. Ratings for each criteria are relative to all samples used to model site PDFs (Fig. 2).
[a] Label for earthquake, tsunami, and (or) disturbance event contact used in original study of site (referenced in Tables S3A-S3G).

Table 3
Statistics for mean PDFs and product PDFs for 16 earthquakes in the maximum rupture model.

Earthquake (Fig. 2)	Unweighted mean PDF					Weighted mean PDF					Product PDF					Recurrence interval (yr)[a]
	mean	1 sigma	2.5–97.5%	median	mode	mean	1 sigma	2.5–97.5%	median	mode	mean	1 sigma	2.5–97.5%	median	mode	
A	1700 CE assumed															
																804
B	800	83	635–930	810	845	804	81	650–930	815	850	813	16	790–855	815	810	
																270
C	1074	127	715–1255	1095	1095	1074	128	715–1255	1105	1125	1098	31	1040–1160	1100	1095	
																196
D	1268	49	1180–1365	1275	1295	1270	43	1190–1345	1280	1295	1282	7	1270–1295	1285	1285	
																205
E	1478	80	1330–1655	1480	1440	1475	75	1340–1640	1475	1440	1474	32	1420–1525	1480	1515	
																95
F	1559	179	1050–1870	1580	1575	1570	148	1185–1855	1580	1575	1576	12	1560–1600	1580	1575	
																843
G	2411	169	2000–2690	2425	2495	2413	155	2090–2680	2420	2335	2424	40	2370–2530	2420	2405	
																446
H	2855	142	2485–3090	2875	2880	2859	146	2465–3095	2880	2880	2880	28	2825–2935	2880	2880	
																363
I	3021	132	2930–3435	3215	3230	3222	126	2965–3455	3230	3230	3213	37	3135–3275	3220	3230	
																285
J	3518	109	3380–3795	3490	3445	3507	105	3380–3785	3480	3445	3475	36	3415–3545	3475	3460	
																396
K	3882	155	3560–4195	3895	3930	3903	150	3580–4200	3920	3975	3859	37	3785–3940	3860	3450	
																225
L	4128	101	3915–4295	4140	4205	4128	101	3915–4295	4140	4205	4147	44	4070–4220	4145	4135	
																291
M	4419	75	4220–4525	4435	4440	4419	75	4220–4525	4435	4440	4441	29	4305–4495	4440	4430	
																121
N	4553	95	4390–4770	4540	4515	4540	95	4370–4770	4530	4520	4535	55	4465–4720	4530	4515	
																577
O	5091	140	4725–5290	5105	5065	5117	120	4810–5295	5125	5065	5122	76	5000–5280	5115	5065	
																829
P	5907	225	5390–6245	5935	5910	5946	221	5420–6255	5985	6005	5926	135	5600–6150	5945	5940	
																578
Q	6549	197	6275–7105	6515	6495	6524	175	6255–7005	6505	6495	6497	71	6360–6635	6500	6495	

All values in calibrated solar years BP.
[a] Difference between means of weighted mean PDFs.

narrowest site PDFs (Biasi and Weldon, 2009; DuRoss et al., 2011). Weighted mean PDFs for each earthquake are shown as gray distributions near the base of Fig. 2 (and on Figs. 4–6, and S4A-S4E); product PDFs are shown in pink. The means of the unweighted mean PDFs, weighted mean PDFs, and product PDFs for post-3-ka earthquakes are within 25 yr of each other; except for earthquake I (192 yr), older means differ by < 53 yr (Figs. 4–6, S4A-S4E; Table 3).

The weighted versions of the mean (summed) earthquake PDFs are the most defensible estimates of the times of earthquakes because they attempt to systematically incorporate the variability in the quality of the dated samples and their probable stratigraphic context relative to the times of earthquakes and tsunamis used to develop the site PDFs (Table 1). To calculate weighted mean PDFs we weight (multiply) each correlated site PDF by the 0–1 weighting factor of Table 2 by averaging the five criteria on which we rate a site PDF prior to summing site PDFs to yield the weighted mean PDF for the 16 earthquakes. Along Utah's Wasatch fault, DuRoss et al. (2011) used a similar 0–1 weighting of site PDFs based on the shape of correlated PDFs.

With their narrower distributions and shorter 95% confidence intervals compared with mean PDFs, are product-PDF confidence intervals reasonable estimates of the uncertainty in the times of the 16 earthquakes in our MRM? To answer this question we consider the degree of coincidence of site PDFs for each earthquake as measured by several indices (Table 1). In calculating product PDFs we assume that all correlated site PDFs for an earthquake are equally valid estimates of the time of the earthquake (Biasi and Weldon, 2009). This is a reasonable assumption for earthquakes C, D, E, F, H, and M, whose site PDFs overlap significantly. The

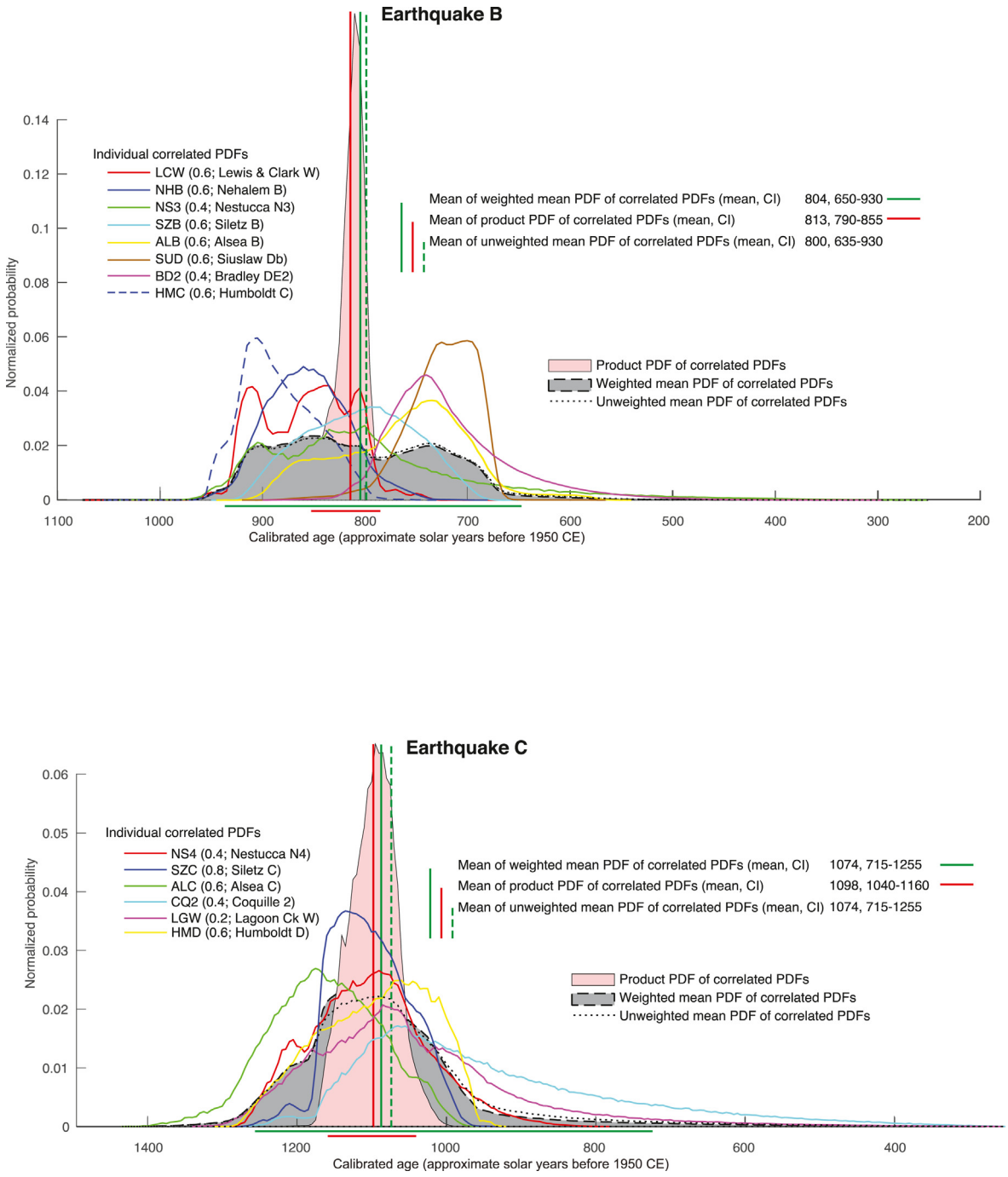

Fig. 4. Correlated site probability density functions (PDFs) for the times of earthquakes (and their tsunamis) B and C. Colored curved lines show the shapes of site PDFs, modeled with OxCal using selected ^{14}C ages (Tables S1 and S3A-S3G) that we assign to the two earthquakes (Table 1). For each site PDF, the quality weighting for that PDF (Table 2; values range from 0.2 to 1) is shown in parentheses followed by the original label for the stratigraphic contact that the PDF dates used in previous studies of that site. Gray shading and black dotted and dashed lines show the unweighted and weighted mean earthquake PDFs (Tables 1 and 3) obtained from summing PDFs for each earthquake (e.g., Biasi and Weldon, 2009; DuRoss et al., 2011). Green vertical lines mark the means of the unweighted and weighted mean PDFs. Pink shading outlines the (unweighted) product PDFs derived from multiplying the site PDFs for each earthquake. Red vertical lines mark the means of product PDFs. Confidence intervals (CI; 95%) for means of PDFs are listed and shown by bars beneath PDFs. Upper green bars beneath PDFs show intervals for weighted mean PDFs; lower red bars for product PDFs. (For interpretation of the references to colour in this figure legend, the reader is referred to the Web version of this article.)

assumption is less likely to be correct, however, for other earthquakes (e.g., B, G, I, K, and for earthquakes with <4 correlated site PDFs) for which one or two site PDFs overlap little with the rest. Most notably, the eight site PDFs for our youngest earthquake (B) are distinctly bimodal (Fig. 4). Mean overlap coefficients also help identify earthquakes with the most consistent site PDFs (Table 1). Chi-squared tests of correlated PDFs for each earthquake, and the similar agreement index (Acomb) for combined site PDFs (OxCal version 4.4; Bronk Ramsey, 2009a), set a high bar for evaluating the overall consistency of product PDFs: of the 16 earthquakes, earthquake B is the only one for which we can reject the null hypothesis that all correlated site PDFs for each earthquake are recording the

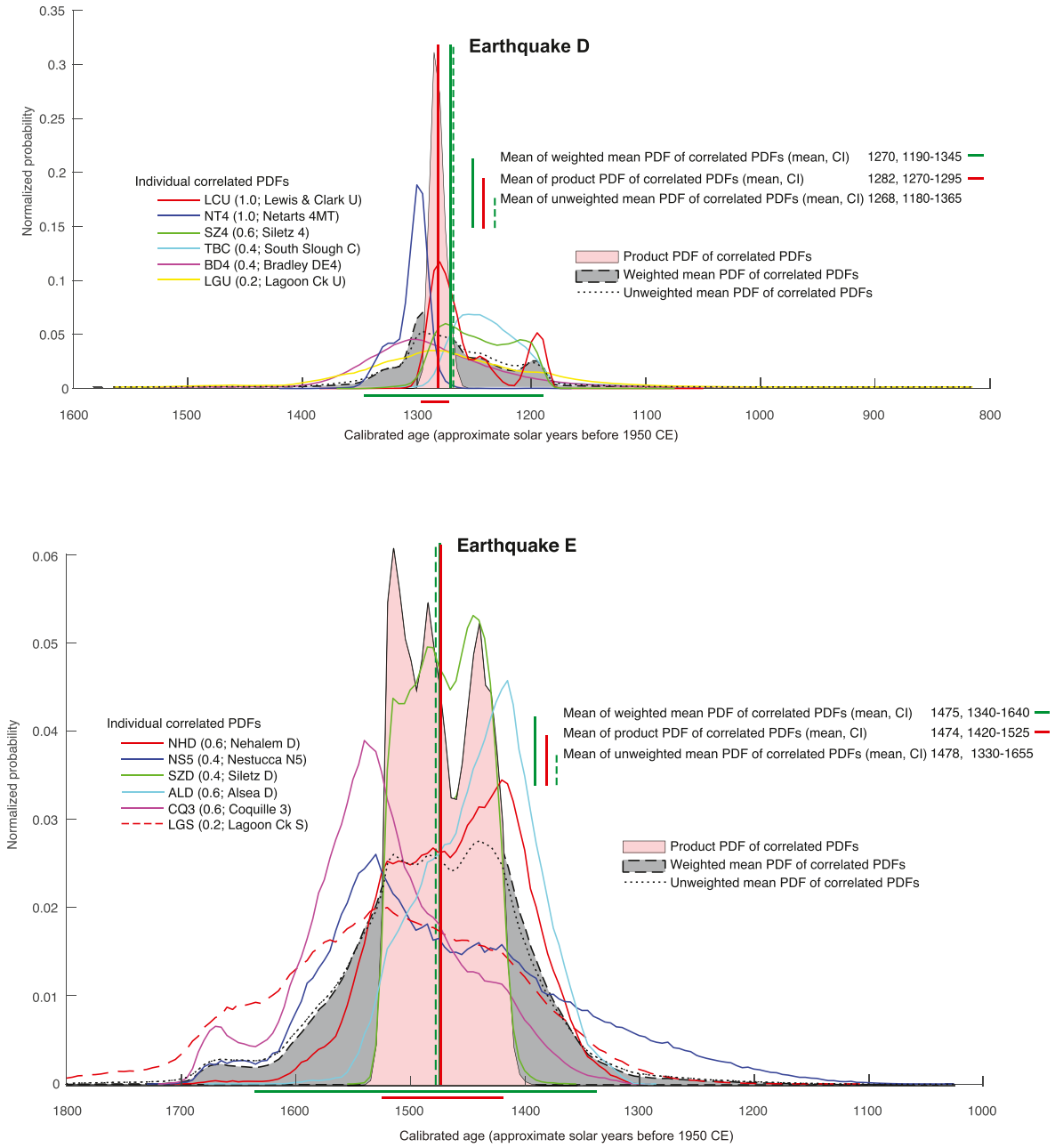

Fig. 5. Correlated site probability density functions (PDFs) for the times of earthquakes (and their tsunamis) D and E. Colored curved lines show the shapes of site PDFs, modeled with OxCal using selected ^{14}C ages (Tables S1 and S3A-S3G) that we assign to the two earthquakes (Table 1). For each site PDF, the quality weighting for that PDF (Table 2; values range from 0.2 to 1) is shown in parentheses followed by the original label for the stratigraphic contact that the PDF dates used in previous studies of that site. Gray shading and black dotted and dashed lines show the unweighted and weighted mean earthquake PDFs (Tables 1 and 3) obtained from summing PDFs for each earthquake (e.g., Biasi and Weldon, 2009; DuRoss et al., 2011). Green vertical lines mark the means of the unweighted and weighted mean PDFs. Pink shading outlines the (unweighted) product PDFs derived from multiplying the site PDFs for each earthquake. Red vertical lines mark the means of product PDFs. Confidence intervals (CI; 95%) for means of PDFs are listed and shown by bars beneath PDFs. Upper green bars beneath PDFs show intervals for weighted mean PDFs; lower red bars for product PDFs. (For interpretation of the references to colour in this figure legend, the reader is referred to the Web version of this article.)

same event at the 95% level (Table 1). Indices that measure the degree of agreement of individual site PDFs with others with which they are combined in OxCal (An, OxCal version 4.4) flag the most discordant PDFs for each earthquake. For example, among the other closely coincident site PDFs for earthquake F, OxCal flags CQ4 as a significant outlier (An = 6%, well below the acceptable value of 60%). Below we discuss why this site PDF is likely hundreds of years older than earthquake F. In any case, sensitivity tests show that removing a single discordant site PDF from the mean PDF or product PDF for any of the post-3-ka earthquakes shifts the means of their mean PDFs or product PDFs by less than a decade.

As we have no reason to suspect that any of the site PDFs for earthquakes C, D, E, F, H, and M differ in the accuracy in which they date these earthquakes, we use the means of the product PDFs for these earthquakes (with their 95% confidence limits) to estimate their age (Table 1; Figs. 2, 4–6, and S4A-S4E). For other earthquakes, whose correlated site PDFs are less coincident, we rely only on the means and 95% confidence limits of their weighted mean

PDFs. Our most precise age intervals are for earthquakes D and F (25 and 40 yr long, respectively) whose product PDFs incorporate 4–5 narrow site PDFs that are tightly restricted with minimum as well as maximum ages (Figs. 5 and 6; Tables S3A-S3F). Intervals for older earthquakes are much less precise (300–840 yr), largely because most are based on weighted mean PDFs restricted with fewer, more imprecise maximum ^{14}C ages. Mean PDFs for earthquakes L, N, O, P and Q are each derived from only two site PDFs (Table 1; Figs. S4C-S4E).

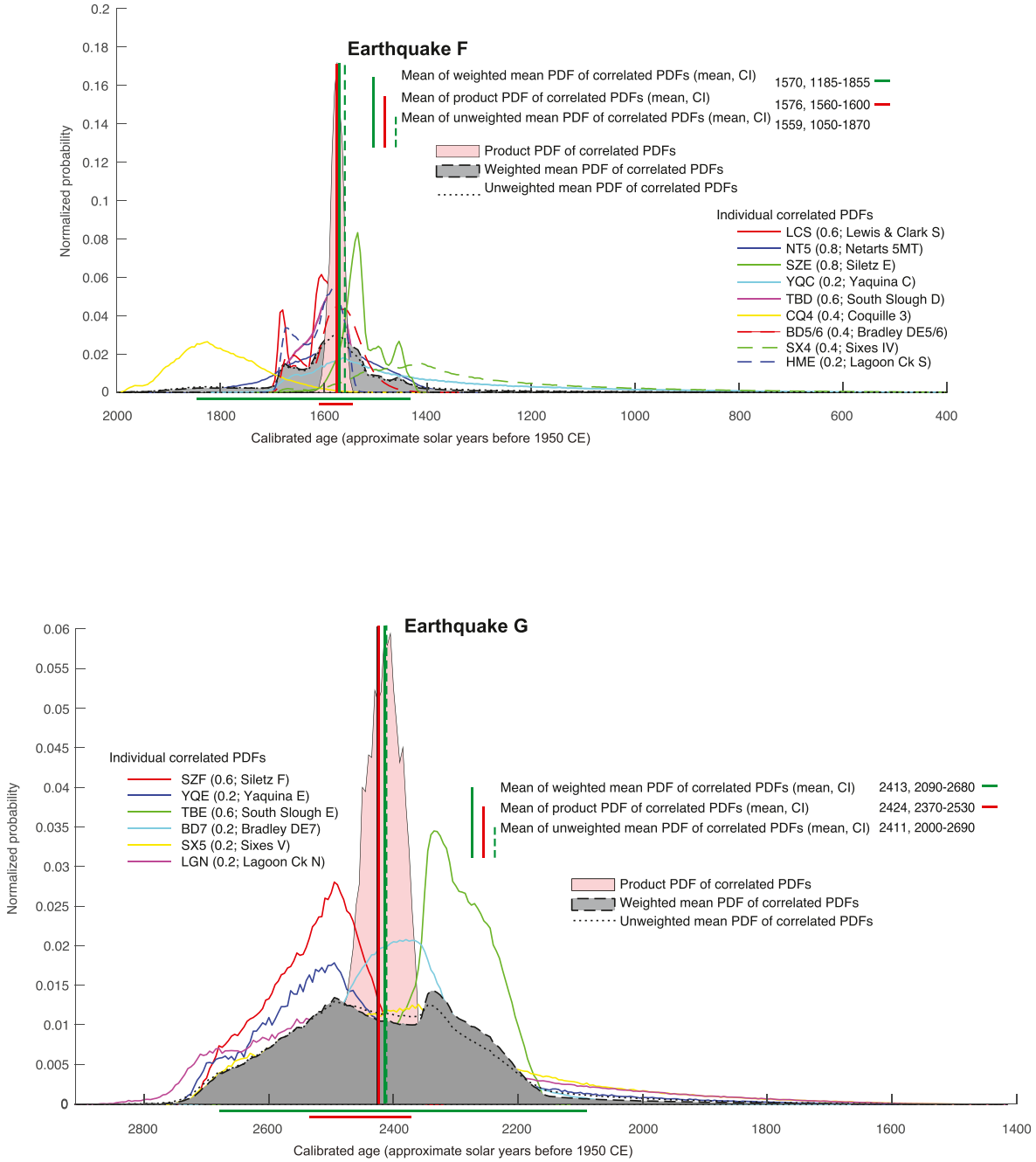

Fig. 6. Correlated site probability density functions (PDFs) for the times of earthquakes (and their tsunamis) F and G. Colored curved lines show the shapes of site PDFs, modeled with OxCal using selected ^{14}C ages (Tables S1 and S3A-S3G) that we assign to the two earthquakes (Table 1). For each site PDF, the quality weighting for that PDF (Table 2; values range from 0.2 to 1) is shown in parentheses followed by the original label for the stratigraphic contact that the PDF dates used in previous studies of that site. Gray shading and black dotted and dashed lines show the unweighted and weighted mean earthquake PDFs (Tables 1 and 3) obtained from summing PDFs for each earthquake (e.g., Biasi and Weldon, 2009; DuRoss et al., 2011). Green vertical lines mark the means of the unweighted and weighted mean PDFs. Pink shading outlines the (unweighted) product PDFs derived from multiplying the site PDFs for each earthquake. Red vertical lines mark the means of product PDFs. Confidence intervals (CI; 95%) for means of PDFs are listed and shown by bars beneath PDFs. Upper green bars beneath PDFs show intervals for weighted mean PDFs; lower red bars for product PDFs. (For interpretation of the references to colour in this figure legend, the reader is referred to the Web version of this article.)

4. Discussion

Our correlation of earthquake PDFs from the 14 coastal sites yields an MRM with 16 megathrust earthquakes since 6.7 ka (events A–Q; Fig. 2). PDFs for earthquakes B, D, F, G, and H, whose correlated site PDFs come from the 7 sites whose stratigraphic records extend to 3 ka, imply ruptures along at least the 500 km of coast between the Columbia River and Humboldt Bay (Table 1). These correlations are consistent with previous estimates of long megathrust ruptures about the times of these earthquakes (e.g., Atwater and Hemphill-Haley, 1997; Kelsey et al., 2002; 2005; Atwater et al., 2004; Goldfinger et al., 2003; 2012; Nelson et al., 2006; 2008; 2020a; Witter et al., 2003; 2012; Priest et al., 2010; Valentine et al., 2012; Peterson et al., 2013; Graehl et al., 2014; Sherrod and Gomberg, 2014; Milker et al., 2016; Hutchinson and Clague, 2017). Matching the means of the weighted mean PDFs for the 16 earthquakes with PDFs for earthquake-induced turbidites is uncertain because turbidites are more frequent. However, the means for earthquakes B, F, L, and P fall near the peaks of PDFs for Goldfinger et al.'s (2012) turbidites T3, T5, T9, and T11, respectively, which are inferred to record full margin ruptures (Fig. 2).

4.1. Do correlated site PDFs for some MRM earthquakes record multiple earthquakes?

Discordant site PDFs for 7 of the 16 earthquakes in our MRM (B, G, I, J, K, L, and P), especially the bimodal distribution for earthquake B, raise this question. Contact HMC at our southernmost site, Humboldt Bay, spans an older age range than other site PDFs included in our correlations for earthquake B (Figs. 2 and 4). Although HMC's PDF almost fails to overlap its nearest correlative at Bradley Lake (contact BD2, coefficient of 0.04), we follow Padgett et al. (2021) in including it with correlations for earthquake B (Table 1) because the PDF for contact HMC significantly overlaps PDFs for contacts LCW (0.92), NHB (0.70), and NS3 (0.49) in northern Oregon. In support of their correlation of contact HMC with others to the north about the time of earthquake B, Padgett et al. (2021) point out that coseismic subsidence across it was less (0.4 ± 0.3 m) than for older contacts at Humboldt Bay (~0.9–1.0 m). This they note, along with similar lesser subsidence measured for some correlative contacts to the north, is still sufficient subsidence to have been produced during a rupture extending many hundreds of kilometers. Contact HMC also largely overlaps the time interval for turbidite T3 (Fig. 2; Padgett et al., 2021), one of the more extensive turbidites studied by Goldfinger et al. (2012). For these reasons, contact HMC is unlikely to record a pre-earthquake-B rupture of limited extent (for example, correlative with the strong shaking without a tsunami of contact BD3 at Bradley Lake).

Despite our efforts to select ^{14}C samples for site PDFs that most closely limit the times of earthquakes, some correlated PDFs that we assign to a single earthquake probably reflect poorly limiting maximum or minimum ages rather than multiple earthquakes closely spaced in time. For example, below we interpret the PDFs for contacts CQ3 and CQ4 at Coquille River to be based on a series of poorly limiting maximum ages, and, therefore, to largely predate earthquakes E and F, respectively (Figs. 2, 5 and 6). In other cases, site PDFs may be overly influenced by poorly limiting minimum ages. PDFs for contact SZ4 at Siletz Bay and TBC at Talbot Creek fall to the younger side of the mean for the product mean PDF for earthquake D (Figs. 2 and 5). Possibilities include that the rooted rhizomes and stems on either side of contact SZ4 used to restrict its PDF are both minimum rather than minimum and maximum ages (Table S3C), that spruce needles yielding an apparent maximum age for contact TBC were thrust into the peat beneath the contact by a toppling tree (e.g., Tables S3D and S3E), or that the other PDFs correlated with earthquake D are more influenced by their maximum rather than their minimum ages. For similar reasons, in our quest to minimize the number of earthquakes in our MRM, for earthquake G we infer that the PDF for contact TBE is largely younger than the contact, and that the PDFs for contacts SZF and YQE are mostly older (Fig. 6). For most older earthquakes (J-Q), all south of Siletz Bay, their modes differ from the means of their weighted mean PDFs (Figs. 2 and S4A-S4E), probably because their site PDFs are fewer, generally broader, and based mostly on maximum ages, which vary widely in how closely they restrict the PDFs to the times contacts formed.

4.2. Evidence for ruptures of limited extent

Although our MRM minimizes the number of ruptures of maximum spatial extent, the site PDFs assigned to earthquakes C and E are most consistent with ruptures of limited extent, and presumably lower magnitude, like some proposed for southern Oregon based on the offshore as well as the onshore record (e.g., Kelsey et al., 2005; Nelson et al., 2006; Goldfinger et al., 2012). Although earthquake C lacks clearly correlative PDFs at Sixes River and Bradley Lake, contact HMD at Humboldt Bay overlaps well with earthquake C's correlatives to the north only as far as Nestucca Bay (Fig. 2). About 20 km farther north at Netarts Bay, Minor and Peterson (2016) infer that an archeological occupation layer, separating two tsunami deposits (insufficiently dated to be included on Fig. 2), represents at least a century. Radiocarbon ages with large uncertainties on charcoal from fire pits above and below the lower tsunami deposit suggest that it was deposited about the times of earthquakes D and C. Atwater et al. (2004), however, reported no tsunami deposit or subsided wetland buried about this time in southwest Washington. If limited to south of Nestucca Bay, earthquake C's rupture may have been <400 km. The PDF for turbidite T3a, inferred by Goldfinger et al. (2012) to record shaking from an earthquake of limited extent, partially overlaps the PDF for earthquake C.

Our other candidate for a rupture shorter than our longest ruptures is earthquake E. Although our site PDFs for earthquakes E and F are too broad to date the earthquakes precisely (or show that they are separate events), at four sites stratigraphic evidence suggests that these events were only decades apart. At Bradley Lake, Kelsey et al. (2005) and Nelson et al. (2006) identified the deposits of two tsunami inundation events about the time of earthquake F, the younger inundation having eroded all or most of the deposits of the older in most lake cores (BD5/6, Fig. 2, Table S1). Nelson et al. (2006) counted ~22 annual varves between the deposits of these inundation events and estimated that minimal erosion during the later event in the most distal part of the lake had removed <20 yr of additional sediment between the deposits of the two events. No attempt was made to try to distinguish the two tsunamis with ^{14}C ages. At Sixes River, 26 km to the south, Kelsey et al. (2002) mapped two extensive earthquake contacts (SX4 and SX3, Fig. 2) about the time of earthquakes E and F, marked by suddenly subsided marsh soils overlain by beds of tsunami-deposited sand and separated by 13–14 cm of tidal mud. Only contact SX4 has a reliable maximum age that we use for its PDF, the other four ages for contacts SX4 and SX3 apparently predate them by hundreds of years (Table S3G). The broad PDF for contact SX4 encompasses the times of both earthquakes (F and E). However, the mud stratigraphically separating contacts SX4 and SX3 represents only decades (Witter and Kelsey, 2004). Although the PDF for contact SX4 has greater overlap coefficients with the adjacent PDFs of earthquake E (0.45–0.57) than with the PDFs for earthquake F (0.22–0.09; Table S4), we include the PDF for contact SX4 in our correlations for earthquake F because

the contact is the lower (older) of the two contacts of about the same age at Sixes River (Fig. 5).

We also infer two earthquakes at about this same time from stratigraphy at two additional sites: Coquille River, 12 km northeast of Bradley Lake, and 210 km farther north at Siletz Bay. At several sites along the Coquille River, Witter et al. (2003) mapped two earthquake-subsidence/tsunami-deposit contacts (CQ3 and CQ4) separated by 0.3–0.5 m of mud and sand, dating from about this time (Witter et al., 2003; Witter and Kelsey, 2004). So as not to leave the PDF for contact CQ4 isolated (discussed above), we correlate contact CQ4 with earthquake F and contact CQ3 with earthquake E (Table 1), implying that both PDFs represent maximum ages for those respective earthquakes. This is a reasonable inference considering the uncertainty in whether or not the minimum age on herb seeds in mud above the contact used for the PDF for contact CQ3 is, in fact, a maximum age (Table S3F). At the Millport Slough locality at Siletz Bay, the modes of the PDFs for earthquake subsidence contacts SZD and SZE, stratigraphically 0.4–0.6 m apart (Witter et al., 2015), differ by less than half a century (Figs. 2, 5 and 6; Table S3C). Despite the uncertainties in interpreting the stratigraphic context of dated macrofossils and the imprecision of the site PDFs correlated with earthquakes E and F at Bradley Lake, Sixes River, Coquille River, and Siletz Bay; based on stratigraphy and the highest quality, most precise limiting ages for these contacts, we suggest that earthquake E occurred ~50 yr after earthquake F. Such a conclusion implies that tidal marshes at these sites may rebuild rapidly following coseismic subsidence, either through rapid postseismic uplift (e.g., Muto et al., 2019) and (or) sedimentation (e.g., Atwater et al., 2001), and be ready to record the next earthquake in less than the ~150 yr previously suggested for some Cascadia tidal sites (e.g., Atwater and Hemphill-Haley, 1997; Atwater et al., 2001; Witter et al., 2003).

4.3. MRM recurrence

Based on our MRM for megathrust earthquakes in central and southern Cascadia, recurrence since 6.7 ka for the 16 earthquakes plus the 1700 CE earthquake is 370–420 yr (95% confidence interval) using product PDFs for earthquakes C, D, E, F, H, and M, and weighted mean PDFs for other earthquakes. This interval is more than a century shorter than the recurrence intervals originally proposed by Kelsey et al. (2002; 480–540 yr) and Witter et al. (2003; 570–590 yr) for southern coastal Oregon, and used by Frankel et al. (2015) to determine overall seismic hazard for this region. The time intervals between individual events vary, however, from the 30–180 yr we infer between earthquakes E and F, to the 400–680 yr and 490–1120 yr intervals between earthquakes A-B and F-G, respectively (Maximum and minimum intervals between these earthquakes are derived from their age ranges on Table 3.). Both of the long gaps are apparent in most coastal records, including those of Atwater et al. (2004) in the Willapa Bay region (Fig. 2). The significant differences in the times between earthquakes result in a coefficient of variation of 0.6–0.9 for earthquakes A-Q at the 95% level. Recurrence for the 6 earthquakes since 1.6 ka (A-F), which includes the most distinct records from all 14 sites, is 260–270 yr, approaching the 240-yr recurrence proposed for southern Cascadia by Goldfinger et al. (2012) based on correlation of marine turbidites.

If earthquakes C and E were, as we infer, less extensive megathrust ruptures closer to magnitude 8 than to magnitude 9, perhaps correlating with smaller turbidites T3a and T4a (Fig. 2), recurrence for greater earthquakes that ruptured all of central and southern Cascadia in the past 3000 yr is 510–540 yr. The mean of this range (530 yr) is near the center of the ranges for Cascadia recurrence proposed over the past three decades (430–600 yr; e.g., Adams, 1990; Atwater et al., 1995; Darienzo and Peterson, 1995; Atwater and Hemphill-Haley, 1997; Goldfinger et al., 2003; 2012; 2016; Atwater et al., 2004; Nelson et al., 2006; Peterson et al., 2013; Graehl et al., 2014; Priest et al., 2017).

Earthquakes prior to 3 ka, such as I, K, and N, may also have had a limited coastal extent (e.g., Witter et al., 2003; Witter and Kelsey, 2004; Witter et al., 2012), but the absence of an older coastal stratigraphic record north of Yaquina Bay makes such inferences speculative. However, the mean PDFs for some of these pre-3-ka earthquakes coincide with the PDFs for turbidites inferred by Goldfinger et al. (2012) to record ruptures of limited extent. Only Bradley Lake, Coquille River, and Sixes River, <40 km apart in southern Oregon, have a record older than 5 ka. For these reasons, we leave the PDF for contact CQ9 uncorrelated with any megathrust earthquake (Fig. 2; Table 1); perhaps it records an earthquake not recorded by subsidence or a tsunami at other coastal sites but which strongly shook Bradley Lake about this time (BD15; Kelsey et al., 2005).

4.4. MRM implications for Cascadia earthquake history

Through their comparison of models of tsunami inundation and megathrust slip budgets near Bradley Lake with the greater number of turbidites inferred to record megathrust earthquakes offshore, Witter et al. (2012; 2013), among others (e.g., Goldfinger et al., 2012; 2016; Priest et al., 2017; Hutchinson and Clague, 2017; Wirth and Frankel, 2019), discuss the many factors that may account for the greater recurrence of megathrust earthquakes along the southern Oregon versus northern Oregon and Washington coasts. While our MRM cannot answer the questions posed by these authors, it does suggest that the ~850-yr gap between earthquakes G and F was followed by a megathrust rupture (earthquake F) extending at least through central and southern Cascadia (>600 km), and that earthquake F was followed ~50 yr later by the more limited rupture of earthquake E (<350 km?). No evidence of two closely spaced earthquakes about this time is reported north of Nehalem River (Atwater et al., 2004; Hutchinson and Clague, 2017) and earthquake E lacks a correlative contact at Humboldt Bay (Fig. 2; Witter et al., 2003; Padgett et al., 2021). First proposed for southern Oregon by Kelsey et al. (2002; 2005) and Witter et al. (2003), such a pattern of a megathrust rupture extending along much of a subduction zone following a long gap of many hundreds of years, and then subsequently followed by a rupture of only hundreds of kilometers is a pattern common at subduction zones (Thatcher et al., 1990; Satake and Atwater, 2007; Seih et al., 2008; Goldfinger et al., 2012, 2013; Witter et al., 2012; Wang et al., 2012; Bilek and Lay, 2018; Clark et al., 2019; Sawai, 2020; Philibosian and Meltzner, 2020). Our MRM is consistent with earthquakes F and E illustrating such a pattern for the central and southern Cascadia subduction zone.

4.5. How can the accuracy and precision of Cascadia's earthquake ages be improved?

Perhaps the greatest improvements will result from continuing efforts to radiocarbon date small (<1 mg), carefully selected macrofossils that provide more closely limiting maximum and minimum ages for earthquake and tsunami contacts (e.g., Kemp et al., 2013; Kelsey and Witter, 2020). Selecting sites specifically for their likelihood of hosting macrofossils that would closely limit ages, such as relatively continuous sections of terrestrial peat containing tsunami deposits correlated with nearby earthquake subsidence contacts (e.g., Schlichting and Peterson, 2006; Peterson and Cruikshank, 2011; Hemphill-Haley et al., 2019), may help. Over the time period during which radiocarbon laboratories reported

the ^{14}C ages that we evaluate, the precision of ages routinely reported by laboratories has increased threefold. This has significantly narrowed age intervals for some earthquakes (D, F, and H), but not for most because of the many uncertainties between the time of death of a macrofossil and the time of an earthquake. However, as our evaluated ages for contacts show (Tables S1 and S3A-S3F), greater numbers of limiting ages for a contact tend to narrow the time gap between maximum and minimum limiting ages. With the decreasing costs of ^{14}C analysis, dating tens of macrofossils per contact is becoming feasible (e.g., Bondevik et al., 1997; Ishizawa et al., 2020). Newer OSL protocols take this approach in using results from the youngest sand grains to date tsunami deposits (discussed above). It should be kept in mind, however, that ^{14}C ages are the product of laboratory analysis statistics: of the 554 ^{14}C ages that we evaluated, 28 likely differ by > 30–220 yr (2 standard deviations) from the time of plant death, and calibration of ages may compound these uncertainties.

Similar improvements in precision and accuracy can be expected from improved methods of Bayesian age modeling of closely limiting ^{14}C ages (Ishizawa et al., 2020). Rather than the single age modeling approach used here, comparing the results of the same types of models using different assumptions, and of different modeling methods (e.g., Parnell et al., 2008; Bronk Ramsey, 2009a; Enkin et al., 2013; Trachsel and Telford, 2017) should lead to greater confidence in earthquake ages (Padgett et al., 2021). Although Padgett et al. (2021) inferred that their ages for three earthquakes at Humboldt Bay (Fig. 2) obtained with a simple OxCal sequence model were the most reliable, including sedimentation rates and perhaps other types of prior information in age-depth models has the potential to greatly improve age precision.

Finally, the advantages of comparing ages obtained by independent dating methods cannot be overstated (Pierce, 1986; McCalpin and Nelson, 2009). Although we failed to independently date tsunami deposits in Bradley Lake because of problematic sand grain lithology, lithologies at other coastal sites may be suitable for OSL or IRSL analyses (e.g., Ishizawaa et al., 2020). Decades ago Atwater et al. (2004) demonstrated that ^{14}C ages on the counted rings of the stumps of trees, inferred to have been killed by earthquake subsidence, could precisely date pre-1700-CE earthquakes. Unfortunately, such stumps that significantly pre-date the 1700 CE earthquake and are accessible in outcrop during the lowest tides have been reported from only two sites in central and southern Cascadia (Nelson et al., 2020a, 2020b).

5. Conclusions

Through correlation of Bayesian age probability density functions (PDFs) based on evaluation of 554 radiocarbon ages for earthquake and tsunamis evidence from 14 coastal sites in central and southern Cascadia, we develop a maximum rupture model (MRM) for 16 great megathrust earthquakes and (or) their tsunamis of the past 6700 yr. Unlike most previous studies, we base our PDFs on the youngest maximum and oldest minimum ^{14}C ages for site evidence. Then, by evaluating the sequence of earthquake PDFs at each site, comparing the degree of temporal overlap of PDFs, and considering stratigraphic evidence at four key sites, we correlate site PDFs along-strike and backward in time to construct an MRM that accounts for all dated evidence with the fewest possible ruptures. Our MRM features four more megathrust earthquakes than previously proposed from coastal evidence in the region. Our attempt to use OSL and IRSL luminescence techniques to confirm ages for tsunami deposits in Bradley Lake, one of Cascadia's longest coastal records, was unsuccessful probably due to fine inclusions of feldspar in analyzed quartz grains.

Average recurrence after 6.7 ka for megathrust earthquakes is 370–420 yr. For the 6 most recent events with the most distinct stratigraphic records from all 14 sites, recurrence after 1.6 ka is 260–270 yr. Two intervals between earthquakes, however, may be ~50 yr, whereas the longest gaps between earthquakes are ~550 and ~850 yr. If earthquakes ~1.1 ka and ~1.5 ka were, as we infer, less extensive ruptures (<400 km), post-3-ka recurrence for the greatest earthquakes whose ruptures extended at least throughout central and southern Cascadia is 510–540 yr. The closely spaced ruptures ~1.6 ka may be an example of a pattern common at subduction zones: a great earthquake rupturing much of the subduction zone following a long gap in ruptures, shortly followed by a rupture of much more limited extent.

To what extent the differences in rupture length and recurrence suggested by our MRM reflect differences in coastal records and in successive megathrust ruptures remain open questions. The completeness of site records of earthquakes and tsunamis in central and southern Cascadia is difficult to evaluate because their creation and preservation thresholds surely differed from earthquake to earthquake and from site to site (Nelson et al., 2006; Witter et al., 2012; Graehl et al., 2014; Shennan et al., 2016). Megathrust ruptures capable of deforming the seafloor and coast adjacent to individual sites also differed in their timing, dimensions, speed, and magnitude along the subduction zone (Wang et al., 2012; Witter et al., 2013; Wang and Trehu, 2016; Priest et al., 2017; Bilek and Lay, 2018; Wirth et al., 2019). Our MRM, like the earlier correlations of Kelsey et al. (2002; 2005) and Witter et al. (2003), is consistent with at least two megathrust earthquakes with less-than-full-margin ruptures in the past 2000 yr. Thus, our MRM supports Frankel et al.'s (2015; Petersen et al., 2020) inclusion of magnitude-8 earthquakes of limited extent in their assessment of regional seismic hazard.

Credit author statement

All authors contributed to interpretation of results and the writing of the paper. Much of the present text reflects the efforts of Nelson, Witter, DuRoss, Kelsey, Engelhart, and Gray. Nelson, Witter, Kelsey, Engelhart, and Padgett did most of the sample preparation, whereas data analysis was largely the work of Nelson, DuRoss, Mahan, and Gray. All authors, except DuRoss, Mahan, and Gray, contributed to fieldwork and the selection of ^{14}C samples.

Declaration of competing interest

The authors declare that they have no known competing financial interests or personal relationships that could have appeared to influence the work reported in this paper.

Acknowledgments

This work was supported by the Earthquake Hazards Program of the U.S. Geological Survey and by U.S. National Science Foundation Awards EAR-1419824 to Horton, EAR-1419844 to Engelhart, and EAR-9405263 to Kelsey. Kelsey, Witter, Engelhart, and Padgett were also funded by the National Earthquake Hazards Reduction Program of the U.S. Geological Survey (Award Numbers 02HQGR0056, 02HQGR0057, G14AP00128, G14AP00129, G17AP00028, G19AP00105, and 1434-93-G-2321). Horton's research was supported by the Earth Observatory of Singapore via its funding from the National Research Foundation Singapore and the Singapore Ministry of Education under the Research Centres of Excellence initiative. Horton was additionally funded by the Singapore Ministry of Education Academic Research Fund (MOE2019-T3-1-004 and MOE2018-T2-1-030). The National Ocean Sciences Accelerator Mass Spectrometry facility (NOSAMS) at Woods Hole

Oceanographic Institution (WHOI) supported the analysis of five ^{14}C AMS samples during Hawkes' WHOI NOSAMS postdoctoral fellowship. Able field and laboratory assistance was provided by Rich Briggs, Lee Ann Bradley, Zeb Maharrey (all with U.S. Geological Survey, Golden, Colorado), Andy Grand Pre (University of Pennsylvania), and SeanPaul La Selle (U.S. Geological Survey, Santa Cruz, California). This manuscript was improved through reviews by Lisa Ely (Central Washington University, Ellensburg, Washington), Kate Clark (GNS Science, Lower Hutt, New Zealand), Chris Goldfinger (Oregon State University, Corvallis, Oregon), and an anonymous reviewer. This work comprises Earth Observatory of Singapore contribution number 355.

Appendix A. Supplementary data

Supplementary data to this article can be found online at https://doi.org/10.1016/j.quascirev.2021.106922 and in two U.S. Geological Survey data releases: Nelson et al. (2020c) and Mahan et al. (2021).

References

Adams, J., 1990. Paleoseismicity of the Cascadia subduction zone—evidence from turbidites off the Oregon-Washington margin. Tectonics 9 (4), 569–583. https://doi.org/10.1029/TC009i004p00569.

Atwater, B.F., 2020. Data from Stratigraphic and Tree-Ring Studies of Late Holocene Earthquakes and Tsunamis at Copalis River, Grays Harbor, Willapa Bay, and Columbia River, Washington and Oregon. U.S. Geological Survey data release. https://doi.org/10.5066/P9GEWF58.

Atwater, B.F., Griggs, G.B., 2012. Deep-sea turbidites as guides to Holocene earthquake history at the Cascadia Subduction Zone—alternative views for a seismic-hazard workshop. U.S. Geol. Surv. Open-File Rep. 2012- 1043, 58. https://doi.org/10.3133/ofr20121043.

Atwater, B.F., Hemphill-Haley, E., 1997. Recurrence Intervals for Great Earthquakes of the Past 3500 Years at Northeastern Willapa Bay, vol. 1576. U.S. Geological Survey Professional Paper, Washington, p. 108. https://doi.org/10.3133/pp1576.

Atwater, B.F., Stuiver, M., Yamaguchi, D.K., 1991. Radiocarbon test of earthquake magnitude at the Cascadia subduction zone. Nature 353 (6340), 156–158. https://doi.org/10.1038/353156a0.

Atwater, B.F., Yamaguchi, D.K., Bondevik, S., Barnhardt, W.A., Amidon, L.J., Benson, B.E., Skjerdal, G., Shulene, J.A., Nanayama, F., 2001. Rapid resetting of an estuarine recorder of the 1964 Alaska earthquake. Geol. Soc. Am. Bull. 113 (9), 1193–1204. https://doi.org/10.1130/0016-7606(2001)113%3C1193:RROAER%3E2.0.CO;2.

Atwater, B.F., Nelson, A.R., Clague, J.J., Carver, G.A., Yamaguchi, D.K., Bobrowsky, P.T., Borgeois, J., Darienzo, M.E., Grant, W.C., Hemphill-Haley, E., Kelsey, H.M., Jacoby, G.C., Nishenko, S.P., Palmer, S.P., Peterson, C.D., Reinhart, M.A., 1995. Summary of coastal geologic evidence for past great earthquakes at the Cascadia subduction zone. Earthq. Spectra 11 (1), 1–18. https://doi.org/10.1193/1.1585800.

Atwater, B.F., Tuttle, M.P., Schweig, E.S., Rubin, C.M., Yamaguchi, D.K., Hemphill-Haley, E., 2004. Earthquake recurrence inferred from paleoseismology. In: Gillespie, A.R., Porter, S.C., Atwater, B.F. (Eds.), The Quaternary Period in the United States, vol. 1. Elsevier Ltd., Amsterdam, pp. 331–350. https://doi.org/10.1016/S1571-0866(03)01015-7.

Atwater, B.F., Musumi-Rokkaku, S., Satake, K., Tsuji, Y., Ueda, K., Yamaguchi, D.K., 2005. The orphan tsunami of 1700. Japanese clues to a parent earthquake in north America. U.S. Geol. Surv. Prof. Pap. 1707 133. https://doi.org/10.3133/pp1707.

Biasi, G.P., Weldon, R.J., 2009. San Andreas Fault rupture scenarios from multiple paleoseismic records: stringing pearls. Bull. Seismol. Soc. Am. 99 (2A), 471–498. https://doi.org/10.1785/0120080287.

Biasi, G.P., Weldon, R.J., , II, Scharer, K., 2011. Rupture length and paleomagnitude estimates from point measurements of displacement—a model-based approach. In: Audemard, M.F.A., Michetti, A.M., McCalpin, J.P. (Eds.), Geological Criteria for Evaluating Seismicity Revisited. Forty Years of Paleoseismic Investigations and the Natural Record of Past Earthquakes, vol. 479. Geological Society of America Special Paper, Boulder, CO, pp. 195–204. https://doi.org/10.1130/2011.2479(09.

Bilek, S.L., Lay, T., 2018. Subduction zone megathrust earthquakes. Geosphere 14 (4), 1468–1500. https://doi.org/10.1130/GES01608.1.

Bondevik, S., Svendsen, J.I., Johnson, G., Mangerud, J., Kaland, P.E., 1997. The Storegga tsunami along the Norwegian coast, its age and run-up. Boreas 26 (1), 29–53. https://doi.org/10.1111/j.1502-3885.1997.tb00649.x.

Bronk Ramsey, C., 2001. Development of the radiocarbon program OxCal. Radiocarbon 43 (2A), 355–363. https://doi.org/10.1017/S0033822200038212.

Bronk Ramsey, C., 2008. Deposition models for chronological records. Quat. Sci. Rev. 27 (1–2), 42–60. https://doi.org/10.1016/j.quascirev.2007.01.019.

Bronk Ramsey, C., 2009a. Bayesian analysis of radiocarbon dates. Radiocarbon 51 (1), 337–360. https://doi.org/10.1017/S0033822200033865.

Bronk Ramsey, C., 2009b. Dealing with outliers and offsets in radiocarbon dating. Radiocarbon 51 (3), 1023–1045. https://doi.org/10.1017/S0033822200034093.

Clark, K.J., Howarth, J., Litchfield, N., Cochran, U.A., Turnbull, J., Dowling, L., Howell, A., Berryman, K.L., Wolfe, F., 2019. Geological evidence for past large earthquakes and tsunamis along the Hikurangi subduction margin, New Zealand. Mar. Geol. 412, 139–172. https://doi.org/10.1016/j.margeo.2019.03.004.

Clague, J.J., 1997. Evidence for large earthquakes at the Cascadia subduction zone. Rev. Geophys. 35 (4), 439–460. https://doi.org/10.1029/97RG00222.

Clarke Jr., S.H., Carver, G.A., 1992. Late Holocene tectonics and paleoseismicity, southern Cascadia subduction zone. Science 255 (5041), 188–192. https://doi.org/10.1126/science.255.5041.188.

Darienzo, M.E., Peterson, C.D., 1995. Magnitude and frequency of subduction-zone earthquakes along the northern Oregon coast in the past 3,000 years. Oregon Geol. 57 (1), 3–12.

Dura, T., Engelhart, S.E., Vacchi, M., Horton, B.P., Kopp, R.E., Peltier, W.R., Bradley, S., 2016. The role of Holocene relative sea-level change in preserving records of subduction zone earthquakes. Curr. Clim. Chang. Rep. 2, 86–100. https://doi.org/10.1007/s40641-016-0041-y.

DuRoss, C.B., Personius, S.F., Crone, A.J., Olig, S.S., Lund, W.R., 2011. Integration of paleoseismic data from multiple sites to develop an objective earthquake chronology. Application to the Weber segment of the Wasatch fault zone. Utah. Bull. Seismol. Soc. Am. 101 (6), 2765–2781. https://doi.org/10.1785/0120110102.

Engelhart, S.E., Horton, B.P., Vane, C.H., Nelson, A.R., Witter, R.C., Brody, S.R., Hawkes, A.D., 2013. Modern foraminifera, δ13C, and bulk geochemistry of central Oregon tidal marshes and their application in paleoseismology. Palaeogeogr. Palaeoclimatol. Palaeoecol. 377 (1), 13–27. https://doi.org/10.1016/j.palaeo.2013.02.032.

Enkin, R.J., Dallimore, A., Baker, J., Southon, J.R., Ivanochko, T., 2013. A new high-resolution radiocarbon Bayesian age model of the Holocene and Late Pleistocene from core MD02-2494 and others, Effingham Inlet, British Columbia, Canada; with an application to the paleoseismic event chronology of the Cascadia Subduction Zone. Can. J. Earth Sci. 50 (7), 746–760. https://doi.org/10.1139/cjes-2012-0150.

Frankel, A., Chen, R., Petersen, M., Moschetti, M., Sherrod, B., 2015. 2014 update of the Pacific Northwest portion of the U.S. National seismic hazard maps. Earthq. Spectra 31 (S1), S131–S148. https://doi.org/10.1193/111314EQS193M.

Galbraith, R.F., Roberts, R.G., 2012. Statistical aspects of equivalent dose and error calculation and display in OSL dating: an overview and some recommendations. Quat. Geochronol. 11, 1–27. https://doi.org/10.1016/j.quageo.2012.04.020.

Garrett, E., Fujiwara, O., Garrett, P., Heyvaert, V.M.A., Shishikura, M., Yokoyama, Y., Hubert-Ferrari, A., Brückner, H., Nakamura, A., De Batist, M., the QuakeRecNankai team, 2016. A systematic review of geological evidence for Holocene earthquakes and tsunamis along the Nankai-Suruga Trough, Japan. Earth Sci. Rev. 159, 337–357. https://doi.org/10.1016/j.earscirev.2016.06.011.

Goldfinger, C., Nelson, C.H., Johnson, J.E., Shipboard Scientific Party, 2003. Deep-water turbidites as Holocene earthquake proxies: the Cascadia subduction zone and northern san andreas fault systems. Ann. Geophys. 46 (5), 1169–1194. https://doi.org/10.4401/ag-3452.

Goldfinger, C., Ikeda, Y., Yeats, R.S., Ren, J., 2013. Superquakes and supercycles. Seismol Res. Lett. 84 (1), 24–32. https://doi.org/10.1785/0220110135.

Goldfinger, C., Nelson, C.H., Morey, A., Johnson, J.E., Gutierrez-Pastor, J., Eriksson, A.T., Karabanov, E., Patton, J., Gracia, E., Enkin, R., Dallimore, A., Dunhill, G., Vallier, T., 2012. Turbidite Event History—Methods and Implications for Holocene Paleoseismicity of the Cascadia Subduction Zone. USGS Professional Paper 1661-F, p. 184. https://doi.org/10.3133/pp1661F.

Goldfinger, C., Galer, S.G., Beeson, J., Hamilton, T., Black, B., Romos, B., Patton, J., Nelson, C.H., Hausmann, R., Morey, A., 2016. The importance of site selection, sediment supply, and hydrodynamics. A case study of submarine paleoseismology on the northern Cascadia margin, Washington, USA. Mar. Geol. 384, 25–46. https://doi.org/10.1016/j.margeo.2016.06.008.

Graehl, N.A., Kelsey, H.M., Witter, R.C., Hemphill-Haley, E., Engelhart, S.E., 2014. Stratigraphic and microfossil evidence for a 4500-year history of Cascadia subduction zone earthquakes and tsunamis at Yaquina River estuary, Oregon, USA. Geol. Soc. Am. Bull. 127 (1–2), 211–226. https://doi.org/10.1130/B31074.1.

Gray, H.J., Mahan, S.A., Nelson, M.S., Rittenour, T.M., 2015. Guide to luminescence dating techniques and their application for paleoseismic research in Western States Seismic Policy Council. Basin and Range Province Seismic Hazard. Summit III, Utah Geol. Surv. Miscell. Publ. 15–5, 18.

Hemphill-Haley, E., Kelsey, H.M., Graehl, N., Casso, M., Caldwell, D., Loofbourrow, C., Robinson, M., Vermeer, J., Southwick, E., 2019. Recent sandy deposits at five northern California coastal wetlands—stratigraphy, diatoms, and implications for storm and tsunami hazards. U.S. Geol. Surv. Sci. Investig. Rep. 2018– 5111, 187. https://doi.org/10.3133/sir20185111.

Huntley, D.J., Lamothe, M., 2001. Ubiquity of anomalous fading in K-feldspars and the measurement and correction for it in optical dating. Can. J. Earth Sci. 38 (7), 1093–1106. https://doi.org/10.1139/cjes-38-7-1093.

Hutchinson, I., Clague, J.J., 2017. Were they all giants? Perspectives on late Holocene plate-boundary earthquakes at the northern end of the Cascadia subduction zone. Quat. Sci. Rev. 169, 29–49. https://doi.org/10.1016/j.quascirev.2017.05.015.

Ishizawa, T., Goto, K., Yokoyama, Y., Goff, J., 2020. Dating tsunami deposits: present knowledge and challenges. Earth Sci. Rev. 200, 102971. https://doi.org/10.1016/j.earscirev.2019.102971.

Johnstone, S.A., Schwartz, T.M., Holm-Denoma, C.S., 2019. A stratigraphic approach

to inferring depositional ages from detrital geochronology data. Front. Earth Sci. 7, 57. https://doi.org/10.3389/feart.2019.00057.
Kelsey, H.M., Witter, R.C., Hemphill-Haley, E., 2002. Plate-boundary earthquakes and tsunamis of the past 5500 years, Sixes River estuary, southern Oregon. Geol. Soc. Am. Bull. 114 (3), 298–314. https://doi.org/10.1130/0016-7606(2002)114%3C0298:PBEATO%3E2.0.CO;2.
Kelsey, H.M., Witter, R.C., 2020. Chapter 30 - radiocarbon dating of tsunami and storm deposits. In: Engel, M., Pilarczyk, J., May, S.M., Brill, D., Garrett, E. (Eds.), Geological Records of Tsunamis and Other Extreme Waves. Elsevier Ltd., Amsterdam, pp. 663–685. https://doi.org/10.1016/B978-0-12-815686-5.00030-4.
Kelsey, H.M., Nelson, A.R., Hemphill-Haley, E., Witter, R., 2005. Tsunami history of an Oregon coastal lake reveals a 4600 yr record of great earthquakes on the Cascadia subduction zone. Geol. Soc. Am. Bull. 117 (7–8), 1009–1032. https://doi.org/10.1130/B25452.1.
Kemp, A.C., Nelson, A.R., Horton, B.P., 2013. 14.31 Radiocarbon dating of plant macrofossils in tidal marsh sediment. In: Schroder, J. (Ed.), Treatise on Geomorphology, vol. 14. Academic Press, Waltham, MA, pp. 370–388. https://doi.org/10.1016/B978-0-12-374739-6.00400-0.
Mahan, S.A., Gray, H.J., Krocyzk, E., 2021. Optical Luminescence Dating of Bradley Lake, Oregon, Tsunami Deposits, Analytical Data for: A Maximum Rupture Model for the Central and Southern Cascadia Subduction Zone—Reassessing Ages for Coastal Evidence of Megathrust Earthquakes and Tsunamis. U.S. Geological Survey data release. https://doi.org/10.5066/P9YWIDOW. In press.
McCalpin, J.P., Nelson, A.R., 2009. Chapter 1 introduction to paleoseismology. In: McCalpin, J.P. (Ed.), Paleoseismology, International Geophysics Series, second ed., vol. 95. Academic Press, Burlington, MA, pp. 1–27. https://doi.org/10.1016/S0074-6142(09)95001-X.
Milker, Y., Nelson, A.R., Horton, B.P., Engelhart, S.E., Bradley, L.-A., Witter, R.C., 2016. Differences in coastal subsidence in southern Oregon (USA) during at least six prehistoric megathrust earthquakes. Quat. Sci. Rev. 142, 143–163. https://doi.org/10.1016/j.quascirev.2016.04.017.
Minor, R., Peterson, C.D., 2016. Multiple reoccupations after four paleotsunami inundations (0.3-1.3 ka) at a prehistoric site in the Netarts Littoral Cell, northern Oregon coast, USA. Geoarchaeology 32 (2), 248–266. https://doi.org/10.1002/gea.21593.
Moernaut, J., VanDaele, M., Fontijn, K., Heirman, K., Kempf, P., Pino, M., Valdebenito, G., Urrutia, R., Strasser, M., DeBatist, M., 2018. Larger earthquakes recur more periodically: new insights in the megathrust earthquake cycle from lacustrine turbidite records in south-central Chile. Earth Planet Sci. Lett. 481, 9–19. https://doi.org/10.1016/j.epsl.2017.10.016.
Murray, A.S., Wintle, A.G., 2003. The single aliquot regenerative dose protocol: potential for improvements in reliability. Radiat. Meas. 37 (4–5), 377–381. https://doi.org/10.1016/S1350-4487(03)00053-2.
Muto, J., Moore, D.P., Barbot, S., Iinuma, T., Ohta, Y., Iwamori, H., 2019. Coupled afterslip and transient mantle flow after the 2011 Tohoku earthquake. Sci. Adv. 5 (9), eaaw1164. https://doi.org/10.1126/sciadv.aaw1164.
Nelson, A.R., 1992. Discordant ^{14}C ages from buried tidal-marsh soils in the Cascadia subduction zone, southern Oregon coast. Quat. Res. 38 (1), 74–90. https://doi.org/10.1016/0033-5894(92)90031-D.
Nelson, A.R., Atwater, B.F., Bobrowsky, P.T., Bradley, L.-A., Clague, J.J., Carver, G.A., Darienzo, M.E., Grant, W.C., Krueger, H.W., Sparks, R., Stafford Jr., T.W., Stuiver, M., 1995. Radiocarbon evidence for extensive plate-boundary rupture about 300 years ago at the Cascadia subduction zone. Nature 378, 371–374. https://doi.org/10.1038/378371a0.
Nelson, A.R., Shennan, I., Long, A.J., 1996. Identifying coseismic subsidence in tidal-wetland stratigraphic sequences at the Cascadia subduction zone of western North America. J. Geophys. Res. 101 (B3), 6115–6135. https://doi.org/10.1029/95JB01051.
Nelson, A.R., Kelsey, H.M., Witter, R.C., 2006. Great earthquakes of variable magnitude at the Cascadia subduction zone. Quat. Res. 65 (3), 354–365. https://doi.org/10.1016/j.yqres.2006.02.009.
Nelson, A.R., Sawai, Y., Jennings, A., Bradley, L., Sherrod, B., Sabean, J., Horton, B.P., 2008. Great-earthquake paleogeodesy and tsunamis of the past 2000 years at Alsea Bay, central Oregon coast, USA. Quat. Sci. Rev. 27 (7–8), 747–768. https://doi.org/10.1016/j.quascirev.2008.01.001.
Nelson, A.R., Hawkes, A.D., Sawai, Y., Horton, B.P., Witter, R.C., Bradley, L.-A., Cahill, N., 2020a. Minimal stratigraphic evidence for coseismic coastal subsidence during 2000 years of megathrust earthquakes at the central Cascadia subduction zone. Geosphere 17 (1), 171–200. https://doi.org/10.1130/GES02254.1.
Nelson, A.R., Hawkes, A.D., Sawai, Y., Engelhart, S.E., Witter, R., Grant-Walter, W.C., Bradley, L.-A., Dura, T., Cahill, N., Horton, B., 2020b. Identifying the greatest earthquakes of the past 2000 years at the Nehalem River estuary, northern Oregon coast, USA. Open Quat. 6 (1), 2–30. https://doi.org/10.5334/oq.70.
Nelson, A.R., Kelsey, H.M., Witter, R.C., 2020c. Core photographs, descriptions, 14C ages, and other supplemental data for Kelsey et al. (2005) and Nelson et al. (2021) about Bradley Lake tsunami history and megathrust earthquake recurrence in the central and southern Cascadia subduction zone. U.S. Geological Survey data release. https://doi.org/10.5066/F7S75DTS.
Ollerhead, J., Huntley, D.J., Nelson, A.R., Kelsey, H.M., 2001. Optical dating of tsunami-laid sand from an Oregon coastal lake. Quat. Sci. Rev. 20 (18), 1915–1926. https://doi.org/10.1016/S0277-3791(01)00043-9.
Padgett, J.S., Engelhart, S.E., Kelsey, H.M., Witter, R.C., Cahill, N., Hemphill-Haley, E., 2021. Timing and amount of southern Cascadia earthquake subsidence over the past 1,700 years at northern Humboldt Bay, California. Geological Society of America Bulletin, USA. https://doi.org/10.1130/B35701.1.
Parnell, A.C., Haslett, J., Allen, J.R., Buck, C.E., Huntley, B., 2008. A flexible approach to assessing synchroneity of past events using Bayesian reconstructions of sedimentation history. Quat. Sci. Rev. 27 (19–20), 1872–1885. https://doi.org/10.1016/j.quascirev.2008.07.009.
Peterson, C.D., Cruikshank, K.M., 2011. Proximal records of paleotsunami runup in barrage creek floodplains from late Holocene great earthquakes in the central Cascadia subduction zone, Oregon, USA. In: Mokhtari, M. (Ed.), Tsunami - A Growing Disaster. IntechOpen Ltd., London, pp. 35–58. https://doi.org/10.5772/24444.
Peterson, C., Clague, J., Carver, G., Cruikshank, K., 2013. Recurrence intervals of major paleotsunamis as calibrated by historic tsunami deposits in three localities: port Alberni, Cannon Beach, and Crescent City, along the Cascadia margin, Canada and USA. Nat. Hazards 68, 321–336. https://doi.org/10.1007/s11069-013-0622-1.
Petersen, M.D., Shumway, A.M., Powers, P.M., Mueller, C.S., Moschetti, M.P., Frankel, A.D., Rezaeian, S., McNamara, D.E., Luco, N., Boyd, O.S., Rukstales, K.S., Jaiswal, K.S., Thompson, E.M., Hoover, S.M., Clayton, B.S., Field, E.H., Zeng, Y., 2020. The 2018 update of the US national seismic hazard model. Overview of model and implications. Earthq. Spectra 36 (1), 5–41. https://doi.org/10.1177/8755293019878199.
Philibosian, B., Meltzner, A.J., 2020. Segmentation and supercycles. A catalog of earthquake rupture patterns from the Sumatran Sunda Megathrust and other well-studied faults worldwide. Quat. Sci. Rev. 241, 106390. https://doi.org/10.1016/j.quascirev.2020.106390.
Pierce, K.L., 1986. Dating methods. In: Wallace, R.E. (Ed.), Active Tectonics: Impact on Society. National Academy Press, Washington, D.C., pp. 195–214
Priest, G.R., Goldfinger, C., Wang, K., Witter, R.C., Zhang, Y., Baptista, A.M., 2010. Confidence levels for tsunami-inundation limits in northern Oregon inferred from a 10,000-year history of great earthquakes at the Cascadia subduction zone. Nat. Hazards 54, 27–73. https://doi.org/10.1007/s11069-009-9453-5.
Priest, G.R., Witter, R.C., Zhang, Y.J., Goldfinger, C., Wang, K.L., Allen, J.C., 2017. New constraints on coseismic slip during southern Cascadia subduction zone earthquakes over the past 4600 years implied by tsunami deposits and marine turbidites. Nat. Hazards 88, 285–313. https://doi.org/10.1007/s11069-017-2864-9.
Satake, K., Atwater, B.F., 2007. Long-term perspectives on giant earthquakes and tsunamis at subduction zones. Annu. Rev. Earth Planet Sci. 35, 349–374. https://doi.org/10.1146/annurev.earth.35.031306.140302.
Satake, K., Wang, K., Atwater, B.F., 2003. Fault slip and seismic moment of the 1700 Cascadia earthquake inferred from Japanese tsunami descriptions. J. Geophys. Res. 108 (B11), 2535. https://doi.org/10.1029/2003JB002521.
Sawai, Y., Namegaya, Y., Okamura, Y., Satake, K., 2012. Challenges of anticipating the 2011 Tohoku earthquake and tsunami using coastal geology. Geophys. Res. Lett. 39 (21), L21309. https://doi.org/10.1029/2012GL053692.
Sawai, Y., 2020. Subduction zone paleoseismology along the Pacific coast of northeast Japan–progress and remaining problems. Earth Sci. Rev. 208, 103261. https://doi.org/10.1016/j.earscirev.2020.103261.
Scharer, K.M., Yule, D., 2020. A maximum rupture model for the southern San Andreas and San Jacinto Faults California, derived from paleoseismic earthquake ages: observations and limitations. Geophys. Res. Lett. 47 (15), e2020GL088532 https://doi.org/10.1029/2020GL088532.
Schlichting, R.B., Peterson, C.D., 2006. Mapped overland distance of paleotsuami high-velocity inundation in back-barrier wetlands of the central Cascadia margin, USA. J. Geol. 114 (5), 577–592. https://doi.org/10.1086/506164.
Sieh, K., Natawidjaja, D.H., Meltzner, A.J., Shen, C.-C., Cheng, H., Li, K.-S., Suwargadi, B.W., Galetzka, J., Philibosian, B., Edwards, R.L., 2008. Earthquake supercycles inferred from sea-level changes recorded in the corals of west Sumatra. Science 322 (5908), 1674–1678. https://doi.org/10.1126/science.1163589.
Shennan, I., Bruhn, R., Barlow, N., Good, K., Hocking, E., 2014. Late Holocene great earthquakes in the eastern part of the Aleutian megathrust. Quat. Sci. Rev. 84, 86–97. https://doi.org/10.1016/j.quascirev.2013.11.010.
Shennan, I., Garrett, E., Barlow, N., 2016. Detection limits of tidal-wetland sequences to identify variable rupture modes of megathrust earthquakes. Quat. Sci. Rev. 150, 1–30. https://doi.org/10.1016/j.quascirev.2016.08.003.
Sherrod, B.L., Gomberg, J., 2014. Crustal earthquake triggering by pre-historic great earthquakes on subduction zone thrusts. J. Geophys. Res. 119 (2), 1273–1294. https://doi.org/10.1002/2013JB010635.
Streig, A.R., Weldon, R.J., II Biasi, G., Dawson, T.E., Gavin, D.G., Guilderson, T.P., 2020. New insights into paleoseismic age models on the northern San Andreas Fault: charcoal inbuilt ages and updated earthquake correlations. Bull. Seismol. Soc. Am. 110 (3), 1077–1089. https://doi.org/10.1785/0120190307.
Thatcher, W., 1990. Order and diversity in the modes of circum-Pacific earthquake recurrence. J. Geophys. Res. 95 (B3), 2609–2623. https://doi.org/10.1029/JB095iB03p02609.
Trachsel, M., Telford, R.J., 2017. All age–depth models are wrong, but are getting better. Holocene 27 (6), 860–869. https://doi.org/10.1177/0959683616675939.
Valentine, D.W., Keller, E.A., Carver, G., Li, W.-H., Manhart, C., Simms, A.R., 2012. Paleoseismicity of the southern end of the Cascadia subduction zone, northwestern California. Bull. Seismol. Soc. Am. 102 (3), 1059–1078. https://doi.org/10.1785/0120110103.
Wang, K., Hu, Y., He, J., 2012. Deformation cycles of subduction earthquakes in a viscoelastic earth. Nature 484, 327–332. https://doi.org/10.1038/nature11032.

Wang, K., Tréhu, A.M., 2016. Invited review paper: some outstanding issues in the study of great megathrust earthquakes—the Cascadia example. J. Geodyn. 98, 1–18. https://doi.org/10.1016/j.jog.2016.03.010.

Wirth, E.A., Frankel, A.D., 2019. Impact of down-dip rupture limit and high-stress drop subevents on coseismic land-level change during Cascadia megathrust earthquakes. Bull. Seismol. Soc. Am. 109 (6), 2187–2197. https://doi.org/10.1785/0120190043.

Witter, R.C., Kelsey, H.M., 2004. Middle to Late Holocene Earthquake Chronologies for the Cascadia Subduction Zone from Two Estuaries in Southern Oregon: Collaborative Research with William Lettis and Associates, Inc., and Humboldt State University. U.S. Geological Survey, National Earthquake Hazards Reduction Program Final Technical Report. Awards 02HQGR0056 and 02HQGR0057), p. 40.

Witter, R.C., Kelsey, H.M., Hemphill-Haley, E., 2003. Great Cascadia earthquakes and tsunamis of the past 6700 years, Coquille River estuary, southern coastal Oregon. Geol. Soc. Am. Bull. 115 (10), 1289–1306. https://doi.org/10.1130/B25189.1.

Witter, R.C., Engelhart, S.E., Nelson, A.R., Milker, Y., Hawkes, A.D., Gao, D., Horton, B.P., Wang, K., 2015. Megathrust Slip Varied during Past Cascadia Subduction Zone Earthquakes at Siletz Bay Central Oregon [abstract]. American Geophysical Union, Fall Meeting, San Francisco abstract no. T11H-08.

Witter, R.C., Hemphill-Haley, E., Hart, R., Gay, L., 2009. Tracking Prehistoric Cascadia Tsunami Deposits at Nestucca Bay, Oregon. U.S. Geological Survey, National Earthquake Hazards Reduction Program Final Technical Report. Award 08HQGR0076), p. 92.

Witter, R.C., Zhang, Y.J., Wang, K., Goldfinger, C., Priest, G.R., 2012. Coseismic slip on the southern Cascadia megathrust implied by tsunami deposits in an Oregon lake and earthquake-triggered marine turbidites. J. Geophys. Res. 117 (B10), B10303. https://doi.org/10.1029/2012JB009404.

Witter, R.C., Zhang, Y.J., Wang, K., Priest, G.R., Goldfinger, C., Stimely, L., English, J.T., Ferro, P.A., 2013. Simulated tsunami inundation for a range of Cascadia megathrust earthquake scenarios at Bandon Oregon, USA. Geosphere 9 (6), 1783–1803. https://doi.org/10.1130/GES00899.1.

Witter, R.C., Briggs, R., Engelhart, S.E., Gelfenbaum, G., Koehler, R.D., Nelson, A.R., La Selle, S.-P., Corbett, R., Wallace, K., 2019. Evidence for frequent, large tsunamis spanning locked and creeping parts of the Aleutian megathrust. Geol. Soc. Am. Bull. 131 (5–6), 707–729. https://doi.org/10.1130/B32031.1.